Progress in Oceanography 181 (2020) 102254

Contents lists available at ScienceDirect

Progress in Oceanography

journal homepage: www.elsevier.com/locate/pocean

Southern Australia Current System based on a gridded hydrography and a high-resolution model

Earl R. Duran[a,*], Helen E. Phillips[b,c], Ryo Furue[d], Paul Spence[a,c], Nathaniel L. Bindoff[b,c,e,f]

[a] Climate Change Research Centre (CCRC), University of New South Wales, Sydney, NSW 2052, Australia
[b] Institute for Marine and Antarctic Studies (IMAS), Hobart, Tasmania, Australia
[c] ARC Centre of Excellence for Climate Extremes (CLEX), Australia
[d] Japan Agency for Marine-Earth Science and Technology (JAMSTEC), Yokohama, Japan
[e] Commonwealth Scientific and Industrial Research Organisation (CSIRO), Australia
[f] Antarctic Climate and Ecosystems Cooperative Research Centre (ACE CRC), Hobart, Tasmania, Australia

ARTICLE INFO

Keywords:
Southern Australia Current System
Shelf break currents
Flinders Current
Transport budget

ABSTRACT

We quantify the annual-mean structure, transport budget and coupling between surface and deep currents along the southern Australian shelves, that we propose be collectively known as the Southern Australia Current System. The system contains eastward Shelf Break Currents (SBC) including the Leeuwin Current Extension, the South Australian Current and the Zeehan Current; and a counter-flowing westward Flinders Current (FC). In this work, we use a high resolution climatological hydrography and a high resolution ocean model forced by an atmospheric climatology.

The westward FC is dual structured with (1) the slope-FC, an undercurrent to the SBC trapped near 600 m depth; and (2) the offshore-FC, a large deep-reaching flow located offshore of the SBC. Along the slanted shelf (not zonally oriented), onshore flows feeding into the FC are weak, and the FC is disconnected from the Tasman Leakage south of Tasmania. Along the zonal shelf, where nearly 80% of total onshore flows occur, the FC intensifies resulting in 12.3 Sv transport at Cape Leeuwin.

The eastward SBC are continuous flows in the upper 250 m. Over steep slopes, downwelling occurs from the SBC into the slope-FC and may be important in maintaining the slope-FC. The Leeuwin Current Extension transport decreases from 1.1 Sv at Cape Leeuwin to 0.1 Sv near the Great Australian Bight due to strong downwelling and offshore exports around Cape Leeuwin. The South Australian Current is weak and steady, and the Zeehan Current increases to 0.4 Sv due to onshore flows stronger than downwelling exports.

We find that the SBC and offshore-FC are coupled through onshore Ekman drift and the SBC and slope-FC are coupled through downwelling. The combined effect is a conversion of widespread northward Ekman drift into downwelling with little impact on the eastward SBC transport. In contrast, the onshore flows feeding into the FC are largely converted into increasing westward FC transport. Even though the Leeuwin Current System off western Australia is fed by geostrophic flows and the Southern Australia Current System is fed by Ekman drift, the annual-mean circulation of the two systems are remarkably similar.

In summer, when the winds are upwelling favourable, the SBC are weaker and partly reversed (to westward). In autumn, the winds become downwelling favourable and the FC is weaker and partly reversed (to eastward). In contrast, the Leeuwin Current System persists annually. The balance mechanism maintaining the seasonal opposition between the SBC and FC warrants further research.

1. Introduction

1.1. Australia's Northern Boundary Currents

The southern continental margin of Australia hosts a unique northern boundary circulation which transports waters between Cape Leeuwin, the southwest corner of Australia, and South East Cape, the southern tip of Tasmania (Fig. 1). Other major boundary currents typically transport water meridionally. The Leeuwin Current flows southward along western Australia and joins the eastward-flowing shelf break currents along southern Australia to form a 5500 km-long boundary current starting from North West Cape (21.8°S) off western

* Corresponding author at: Climate Change Research Centre, Level 4 Mathews Building, The University of New South Wales, Sydney NSW, 2052, Australia.
E-mail address: earl.r.duran@gmail.com (E.R. Duran).

https://doi.org/10.1016/j.pocean.2019.102254
Received 19 July 2018; Received in revised form 18 December 2019; Accepted 20 December 2019
Available online 07 January 2020
0079-6611/

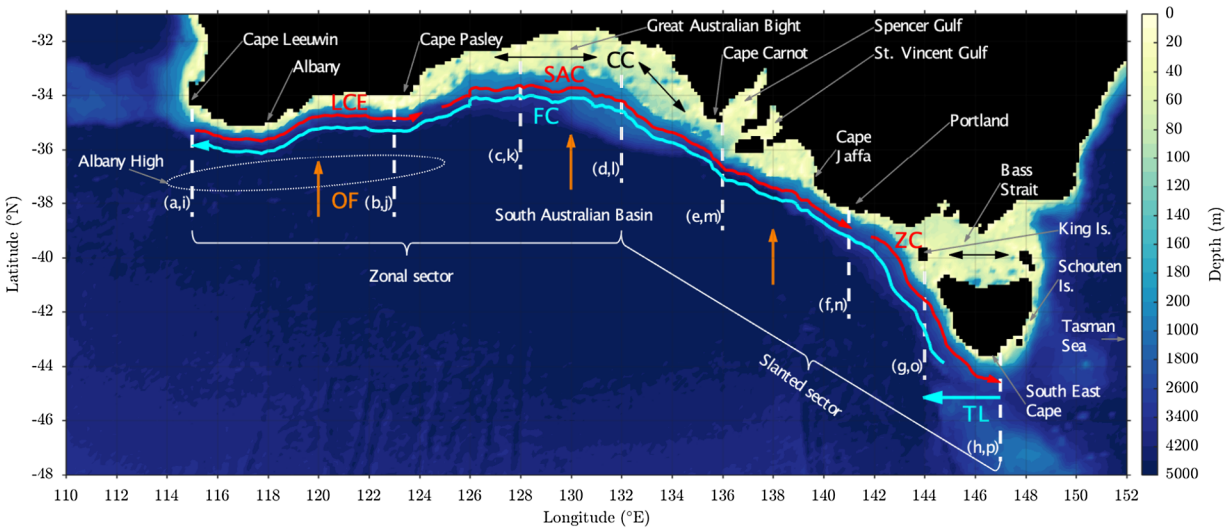

Fig. 1. Southern Australian bathymetry (shadings, the colour increment changes from 10 m to 400 m at 200 m) from Smith and Sandwell (1997) bin averaged onto the CARS grid, important land forms and locations (indicated by small gray arrows), major currents or flows (larger coloured arrow) and location of cross-sections for latitude versus depth plots (white dashed lines). LCE (red arrow): Leeuwin Current Extension. SAC (red arrow): South Australian Current. ZC (red arrow): Zeehan Current. FC (cyan arrow): Flinders Current. TL (cyan arrow): Tasman Leakage. OF (orange arrows): onshore flows. CC (black arrows): coastal currents. (For interpretation of the references to colour in this figure legend, the reader is referred to the web version of this article.)

Australia to South East Cape, Tasmania (43.6°S). These surface currents represent the longest boundary circulation in the world (Middleton and Bye, 2007; Ridgway and Condie, 2004).

Ridgway and Condie (2004) proposed the following naming convention for the surface circulation over the southern Australian shelf break. The Leeuwin Current Extension is the eastward continuation of the poleward Leeuwin Current which pivots anticlockwise around Cape Leeuwin (115°E) and continues eastward until Cape Pasley (124°E), the western edge of the Great Australian Bight (Ridgway and Condie, 2004; Batteen et al., 2007). The South Australian Current emerges within the Great Australian Bight and flows over the shelf break eastward then south-eastward out of the Bight, past the shallow Spencer and St. Vincent Gulfs, and as far south as Portland (141°E). The Zeehan Current forms west of the Bass Strait, flows poleward along the western Tasmanian shelf and tips eastward around South East Cape (147°E, Oliver and Holbrook, 2018). This series of currents together forms a continuous surface flow that we call here the Shelf Break Currents (SBC). Middleton and Cirano (2002) described the slope circulation underneath and south of the SBC. The Flinders Current (FC) flows westward from western Tasmania to Cape Leeuwin. This current has a larger width and depth range and flows in the opposite direction to the SBC.

The continental margin topography displays varying steepness (Fig. 1), which has implications for boundary current structure. For example, at the shelf break, steep topography may reduce ocean-shelf exchange (Huthnance, 1995) but produce a more coherent alongshore current (Pennel et al., 2012). Here, changes in steepness mainly occur across the Great Australian Bight, delimited by Cape Pasley and Cape Carnot. Inside the Bight, the shallow shelf is wider and the continental slope is less steep, especially on the eastern side where isobaths between 200 m and 2000 m are widely spaced. Over Bass Strait, the open, shallow shelf provides a connection between the South Australian Basin and the Tasman Sea. These shallow shelf regions provide a wide platform for shallow coastal currents to exist and interact with the shelf break currents. Outside these regions, the continental margin is characterised by a narrow shelf and steep slope giving a sharp shelf break.

From west to east, the margin orientation also shifts from zonal to slanted along a northwest-to-southeast tilt. This has implications for current trapping against the shelf. For example, Middleton and Cirano (2002) applies western boundary current theory at the northern boundary (i.e. zonal shelf) south of Australia to describe the FC. Along the slanted shelf however, eastern boundary current theory (e.g. McCreary et al., 1993) may apply to describe the FC because the shelf here is facing west. Here, the "zonal sector" includes the Leeuwin Current Extension and the South Australian Current's west half, which flow approximately zonally until the eastern Great Australian Bight near 132°E. East of this, the "slanted sector" includes the South Australian Current's east half and the Zeehan Current, which flow south-eastward along a northwest-to-southeast slant.

1.2. The shelf break currents

Evidence that the Leeuwin Current rounds Cape Leeuwin and continues eastward into the Great Australian Bight is widespread. These include observations of pelagic and demersal (living close to the floor) fauna of tropical origin being found in the Great Australian Bight (Garrey et al., 1981), satellite temperature observations (Legeckis and Cresswell, 1981) and estimates of steric height along the eastern Indian Ocean (Godfrey and Ridgway, 1985). A Lagrangian study also quantified the Leeuwin Current transport as it travels poleward and turns east towards the Great Australian Bight (Yit Sen Bull and van Sebille, 2016). The warm and relatively high salinity Leeuwin Current Extension can reach speeds greater than 100 cm s^{-1} over the 200 m isobath (Cresswell and Peterson, 1993) and has a mean speed of 50 cm s^{-1} down to 250 m (Cresswell and Griffin, 2004). The Leeuwin Current Extension is periodically weakened (enhanced) by large anticyclonic eddies (small cyclonic eddies) in the region between Cape Leeuwin and Albany, as shown from surface drifter track measurements (Godfrey et al., 1986) and an eddy tracking study (Cresswell and Griffin, 2004).

The South Australian Current contains warm and very high salinity waters originating from the centre of the Great Australian Bight (Rochford, 1986) and the Spencer and St. Vincent's Gulfs (Godfrey et al., 1986). The current flows south-eastward over the shelf break to western Bass Strait (Ridgway and Condie, 2004) and can reach speeds of 50 cm s^{-1} down to 200 m (Middleton and Bye, 2007). The Zeehan Current is a poleward current found over the western shelf break of Bass Strait and the western and southern shelf breaks of Tasmania (Baines et al., 1983; Thompson and Veronis, 1983). It is a relatively warm and salty current, fed by the South Australian Current, with current speeds reaching 40 cm s^{-1} down to 300 m (Ridgway, 2007). Near the southern tip of Tasmania, the Zeehan Current meets the counter-flowing East

Australian Current Extension, which flows poleward along the eastern shelf break of Tasmania and pivots westward towards South East Cape (Cresswell, 2000; Oliver and Herzfeld, 2016).

1.3. The deep-ocean circulation

The FC is the northern branch of the south-eastern extension of the Indian Ocean subtropical gyre (Hufford et al., 1997; McCartney and Donohue, 2007). The FC emerges off western Tasmania, flows westward to the south-west corner of Australia and is found between the surface and 2000 m (Middleton and Cirano, 2002). The FC is located beneath the SBC along the continental slope and extends to the sea surface south of the SBC. Observational data show the FC strengthens and shoals east to west with a mean speed of 4 cm s^{-1} near 1000 m depth west of Tasmania, 3–7 cm s^{-1} between 500 and 900 m near Portland (Middleton and Bye, 2007), and 20 cm s^{-1} between 400 and 600 m near Albany (Cresswell and Peterson, 1993).

Middleton and Cirano's (2002) numerical experiments showed permanent positive wind-stress curl in the South Australian Basin leads to regional northward barotropic Sverdrup transport that is deflected westward along the southern Australian margin, resulting in the FC. We note that Sverdrup theory may not explain the northwestward-flowing part of the FC along the slanted coast (east of 132°E), because it is along an eastern boundary (McCreary, 1981; McCreary et al., 1991) and should be eliminated by the offshore propagation of Rossby waves (Anderson, 1975). It is therefore possible that the slanted part of the FC is maintained by another mechanism.

In addition to the broad, northward Sverdrup flow, the FC may be fed by recirculating flows in the South Australian Basin. A sea-surface height summer average (Middleton and Platov, 2003) revealed the "Albany High" (Middleton and Bye, 2007), a large quasi-stationary anticyclonic eddy centred off Albany. Here, the FC is the northern westward-flowing arm of the Albany High. The southern eastward-flowing arm coincides with a transport field estimated using hydrographic and direct-velocity measurements from McCartney and Donohue (2007).

A further potential source of water to the FC is the Tasman Leakage, which carries water from the Pacific Ocean around southern Tasmania (Fig. 1). The FC is sometimes referred to as an extension of the Tasman Leakage because part of the Tasman Leakage flows northwestward towards the coast (Feng et al., 2016; Middleton and Cirano, 2002; Rosell-Fieschi et al., 2013), although other studies have shown most of Tasman Leakage flows westward away from the shelf into the South Australian Basin interior (Speich et al., 2002; van Sebille et al., 2012; van Sebille et al., 2014).

1.4. Present research

Understanding the structure and the water transport of these boundary currents is essential as they constitute a platform for carrying Indian Ocean waters from the Leeuwin Current eastward via the SBC, and Pacific Ocean waters from the Tasman Leakage south of Tasmania westward via the FC. Yet, the currents are known only from drift tracking measurements (Godfrey et al., 1986; Cresswell and Griffin, 2004), cross-shore sections (Cresswell and Peterson, 1993), sea surface height and sea surface temperature maps inferred from satellite data (Legeckis and Cresswell, 1981; Ridgway and Condie, 2004) and high-resolution model experiments (Middleton and Cirano, 2002; Middleton and Platov, 2003; Cirano and Middleton, 2004; Batteen and Miller, 2009). While these studies provide insight into parts of the circulation, summarised in Middleton and Bye's (2007) review, there is no comprehensive analysis of the three-dimensional structure and transport budget of the boundary circulation as a whole. In particular, the SBC and FC coupling is still poorly understood. In the present paper, we provide the first three-dimensional geostrophic velocity field along Australia's southern boundary purely from observations, and support these results with a parallel analysis of a high-resolution model simulation. Given that the Great Australian Bight sustains one of the largest fisheries in Australia (McClatchie et al., 2006), our three-dimensional transport budget can provide clues to better understand sources for primary productivity in the region (e.g. Cetina-Heredia et al., 2018).

In this study we consider the SBC and FC as a system of currents and provide a complete description of their transport and the exchanges between them, following Furue et al.'s (2017) methodology that was applied to the Leeuwin Current System along western Australia. The approach we take is to

- examine the currents' long-term mean, three-dimensional structure reconstructed from both a high-resolution gridded hydrography and an eddy-resolving ocean general circulation model forced by an atmospheric climatology;
- determine the SBC and FC annual-mean transport as they travel zonally along southern Australia, the lateral transports feeding into them, and their vertical transport exchanges;
- examine the coupling between the SBC and FC in the annual-mean and present an overview of the currents' seasonality.

Here, we propose that the circulation off southern Australia, comprising the SBC, FC, coastal currents (over the shallow shelf) and onshore flows (from the ocean interior), be known, collectively, as the Southern Australia Current System.

The next section provides a description of the datasets (Section 2.1), the derivation of mass-conserving geostrophic velocities (Section 2.2), the volume definition of the SBC and FC (Section 2.3), and the derivation of a Southern Australia Current System transport budget (Section 2.4). Section 3 describes the three-dimensional structure of the system in Section 3.1, the transport budget in Section 3.2 and the SBC and FC coupling and seasonality in Section 4.3. Finally, Section 4 summarizes the analysis and presents a closing discussion.

2. Methodology

2.1. Datasets

CARS-Aus8, which we call CARS, is a 1/8°-resolution climatology of ocean temperature and salinity around Australia gridded over 79 vertical levels (Ridgway et al., 2002; http://www.marine.csiro.au/atlas/). These levels are distributed over 5500 m depth with thin levels in the upper 100 m depth and thicker levels with increasing depth. The density of observations fed into CARS is high near the coast due to a large number of hydrographic measurements there (Ridgway et al., 2002). The density decreases offshore but still provides a reasonable amount of approximately spatially uniform observations due to data collected by the Argo array. The "Aus8" version of CARS includes observations up to 2012 (see Duran, 2015 and http://www.marine.csiro.au/atlas/ for more details). Hydrographic profiles are mapped onto the grid through an adaptive four-dimensional interpolation technique which differs from other interpolation methods as it considers land barriers and varying topography over continental margins (Ridgway et al., 2002). Hence the interpolation technique better incorporates coastal flow structures over continental margins (Ridgway et al., 2002). For example, in the ocean interior, the interpolation technique uses a weighted least squares quadratic filter (loess filter, Cleveland and Devlin, 1988) which selects nearby observations within a circle. Near the coast, in regions of shallower bathymetry, the loess filter captures data within an ellipse elongated along the isobaths. This interpolation technique narrows the data selection across isobaths and is essential to resolve boundary currents, which are strongly constrained by topography. Due to these properties, the coastal currents are revealed in our geostrophic calculations (see Section 2.2). The interpolation technique also purposefully creates artificial ocean data underneath the bathymetry to allow the end-user to apply their own topography mask. In the

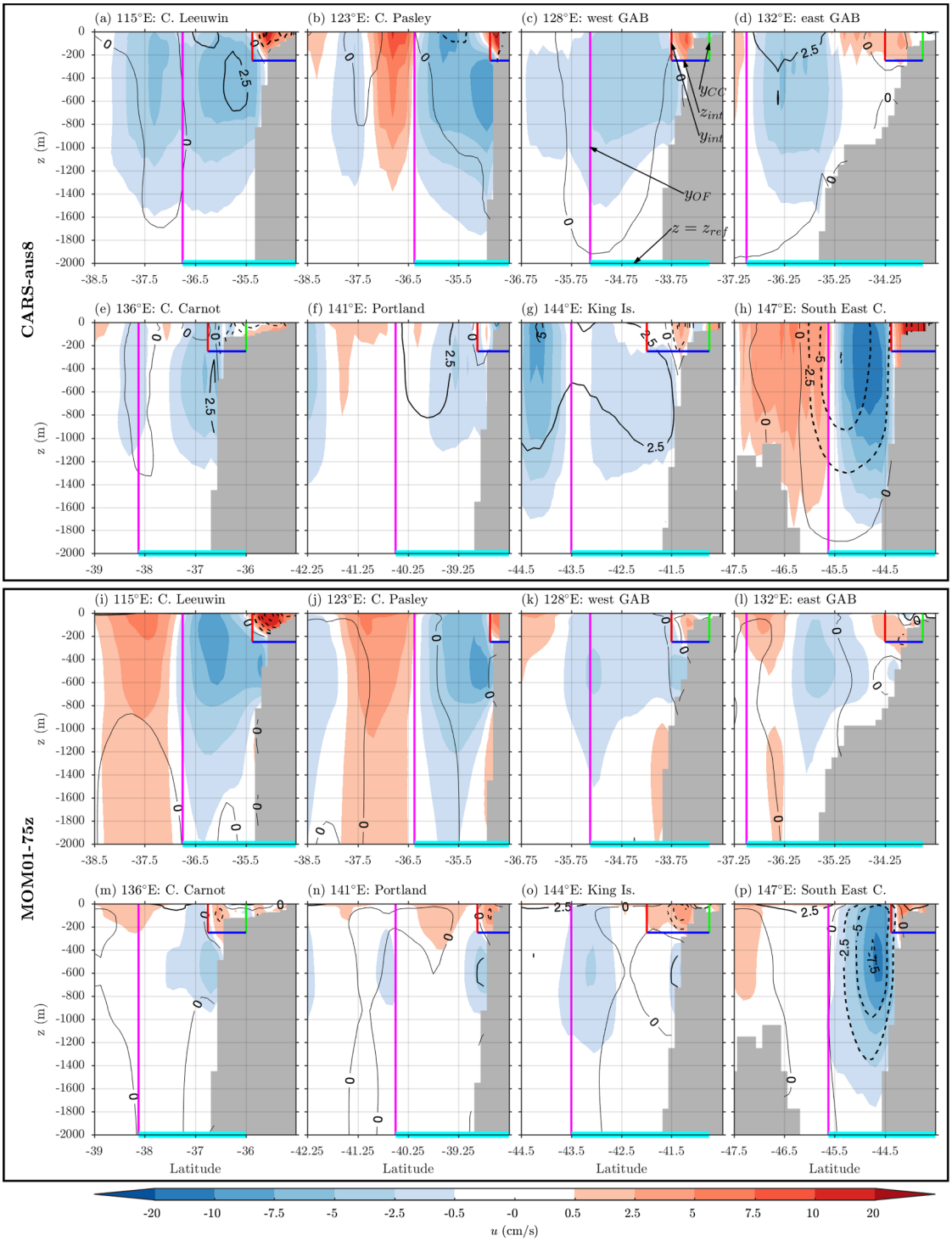

Fig. 2. Meridional sections along southern Australia of (a-h) geostrophic velocities in CARS and (i-p) full velocities in MOM01. Zonal geostrophic velocities u_g in CARS (full zonal velocities in MOM01) in cm s^{-1} (shadings, non-monotonic scale) and meridional geostrophic velocities v_g in CARS (full meridional velocities in MOM01) in cm s^{-1} (contours, every 2.5 cm s^{-1}, thick solid lines show positive values, thick dashed lines show negative values, thin solid lines show zero contour). Boundaries of the SBC and FC as follows: (green) is the SBC north boundary; z_{int} (blue) is the SBC bottom boundary and the FC top boundary; y_{int} (red) is the SBC south boundary and the FC north boundary; y_{OF} (magenta) is the FC south boundary; z_{ref} (thick cyan) is the FC bottom closed boundary at the reference depth. (For interpretation of the references to colour in this figure legend, the reader is referred to the web version of this article.)

present work we choose the 2-minute (1/30° resolution) version of Smith and Sandwell (1997) bathymetry bin-averaged onto CARS grid. The annual mean, and annual and semi-annual harmonics are determined by fitting at each grid point. In the present study, we use only the annual-mean component.

Ridgway et al. (2002) validated CARS against independent data and found that CARS consistently agrees with satellite and in-situ sea surface temperature products and represents the general features of the annual amplitude and phase (for the seasonal variability). Salinity fronts were much better represented in CARS than in another traditional climatology, particularly in boundary current regions. Uncertainty maps indicate CARS sea surface temperature within the

Australasian region is within the ±0.5° range (Ridgway et al., 2002). Within this difference pattern, there are coherent large-scale features and more intense small-scale structures near the shelf. Near the shelf, they found inappropriately short spatial scales occur when the observations fed into CARS are heavily non-spatially uniform and form clusters of close-packed data separated by data poorer or voided areas. These tend to allow the formation of inappropriately short spatial scales from one cluster to the next. This caveat is further discussed when we next introduce the model used in this study.

To include Ekman drift in the CARS transport budget analysis, we use wind stress from ERA-Interim gridded reanalysis (Dee et al., 2011) averaged over 2003–2012. We choose a period corresponding to the final decade of CARS sampling when the number of observations in the upper 2000 m is dramatically increased due to the global Argo array launch in 2000. In general, ERA-Interim winds are stronger between 30 and 60° S than satellite winds from QuikSCAT (Chaudhuri et al., 2013), meaning that wind-driven Ekman drift derived from ERA-Interim may be stronger than that from satellite observations.

MOM01 is a 1/10°-resolution ocean model using the MOM5 code (Griffies, 2012) and providing non-assimilated temperature, salinity and velocity fields gridded over 75 vertical levels (Stewart et al., 2017). Similar to CARS, these levels are thin near the surface and increase in thickness with increasing depth. The model is global and forced by CORE2-NYF, a repeated climatological annual cycle of sea-surface atmospheric forcing with six hourly synoptic variability (Large and Yeager, 2009). MOM01 is forced under this cycle for 108 years and we select the last 7 years to produce our equilibrated mean ocean state. In Section 3.2, we use the temperature and salinity fields in MOM01 to calculate geostrophic velocity (see Section 2.2) and briefly discuss how the MOM01 transport budget derived from geostrophic velocity compares with the budget derived from the full model velocity.

In Section 3.1 we find that CARS shows some minor artificial fragmentation in the currents which we briefly discussed above citing Ridgway et al. (2002). Our high resolution model, however, produces a coherent current system. In addition to this, the prescribed climatological forcing applied to the model results in a numerical simulation of a mean and seasonal cycle that is well suited for comparison with an observational climatology like CARS. We note that, as for ERA-Interim winds, the winds in CORE2-NYF, which are based on the NCEP reanalysis, are generally stronger than satellite winds from QuikSCAT (Large and Yeager, 2009). However, in the Southern Hemisphere, the westerlies are slightly stronger in ERA-Interim than in CORE2-NYF, particularly around 50° S (Chaudhuri et al., 2013).

2.2. Geostrophic velocity derivation

Since the FC can extend as deep as 2000 m (Middleton and Cirano, 2002), we choose a reference depth of $z_{\text{ref}} = -2000$ m, which is also the depth limit of Argo observations. We note the annual-mean density field in CARS and MOM01 agree reasonably well everywhere, except near Albany where CARS shows lighter surface densities (not shown), which would result in a higher Albany High and a locally stronger FC in CARS.

To compute geostrophic velocities in regions shallower than the reference depth, we apply the Helland-Hansen method (Helland-Hansen, 1934; Fomin, 1964). This method states velocities at the bottom of a land portion shallower than the reference depth are zero. This method and Ekman drift calculation are set out in Appendix A.1. A drawback of the Helland-Hansen method is that it produces unphysical vertical flows across the sea bottom over the margin, which introduces error in three-dimensional transport budgets. To eliminate this deficiency, and obtain a three-dimensional transport budget that closes to computer precision, we apply the Zero-Divergence method described in Furue et al. (2017) and here in Appendix A.2.

2.3. SBC and FC definition

To calculate the Southern Australia Current System transport budgets we define two control volumes, one around the SBC and the other around the FC. These boundaries are defined by visually inspecting meridional sections in CARS. We then apply the same boundaries in MOM01 to keep consistent volumes in our calculations.

We first inspect meridional sections at the locations shown in Fig. 1 (black dashed lines) to find the currents' vertical structure and position relative to the margin (Fig. 2a-h). The reader can also compare CARS sections with MOM01 sections, which use full model velocity (Fig. 2i-p). Since the coastline orientation varies as the currents progress zonally, we consider both zonal and meridional flow components to help identify the currents. Therefore, in Fig. 2 we present the zonal component as shading and the meridional component as contours. The longshore currents can be clearly identified in the zonal velocity up until Cape Carnot at 136°E (Fig. 2e). Further east, the meridional velocity helps to identify the currents.

While the SBC are relatively narrow, thin and well contained along the shelf break, the FC is wider and thicker, with a varying core position. We define here an "offshore-FC" south of the SBC, centered at the surface and extending to 2000 m depth (Fig. 2a sub-surface "slope-FC" centered at 600 m underneath the SBC and adjacent to the slope (Fig. 2pe-FC forms a core that is clearly separate from the offshore-FC in MOM01 (Fig. 2i-o). Hence, the SBC and FC volumes can be defined by separating the water column into an upper layer containing the SBC and upper offshore-FC, and a lower layer containing the slope-FC and lower offshore-FC. The horizontal interface z_{int} between the upper and lower layers is therefore the SBC bottom boundary. We choose $z_{\text{int}} = -250$ m (Fig. 2, blue line) as this level is generally very close to, or within, the 0 to 4 cm s^{-1} eastward velocity range at the SBC base. $\mathbf{V}_{\text{up}}$ (Fig. 3a) is the integral of geostrophic velocities from the surface to z_{int} plus Ekman drift and $\mathbf{V}_{\text{low}}$ (Fig. 3b) is the integral of geostrophic velocities from z_{int} to z_{ref}; hence

$$\mathbf{V}_{\text{up}}(x, y) = \int_{z_{\text{int}}}^{0} \mathbf{V}_{\text{g}}\, dz + \mathbf{V}_{\text{ek}} \tag{1}$$

$$\mathbf{V}_{\text{low}}(x, y) = \int_{z_{\text{ref}}}^{z_{\text{int}}} \mathbf{V}_{\text{g}}\, dz. \tag{2}$$

These depth integrated velocity fields produce transports per unit width in $m^2 s^{-1}$. Note that $\mathbf{V}_{\text{up}}$ and $\mathbf{V}_{\text{low}}$ from MOM01 are shown in Fig. 3c,d. In this case we simply used full model velocity integrated in the upper and lower layers, rather than the sum of geostrophic and Ekman velocities. In MOM01, the full model velocities in the SBC and FC are generally stronger than the sum of geostrophic and Ekman velocities (not shown). Therefore the MOM01 full SBC and FC transport will be stronger than MOM01 geostrophic transport (see Section 3.2).

We present in Fig. 4 a Southern Australia Current System three-dimensional schematic diagram to understand transport budget exchanges. This schematic illustrates the SBC eastward transport (U_{SBC} thick light blue arrow) and FC westward transport (U_{FC} thick light yellow arrows), which includes the slope-FC below the SBC, and the offshore-FC upper and lower parts. Inward/outward transports into or out of the SBC or FC are indicated as thin coloured arrows. Here, an increase in SBC transport can be supplied from three sources: southward coastal current inflows (V_{CC} thin green arrows), northward upper offshore-FC inflows (V_{SBC} thin red arrows), and slope-FC upwelling (W_{SBC} thin blue arrows). Similarly, an increase in FC transport can be supplied by three sources: southward SBC inflows into the upper offshore-FC (V_{FC} thin red arrows), SBC downwelling into the slope-FC (W_{FC} thin blue arrows), northward ocean interior onshore flows into the offshore-FC (V_{OF} thin magenta arrows).

The SBC and FC control volume boundaries are shown in meridional sections of velocities (Fig. 2) and maps of depth integrated velocities

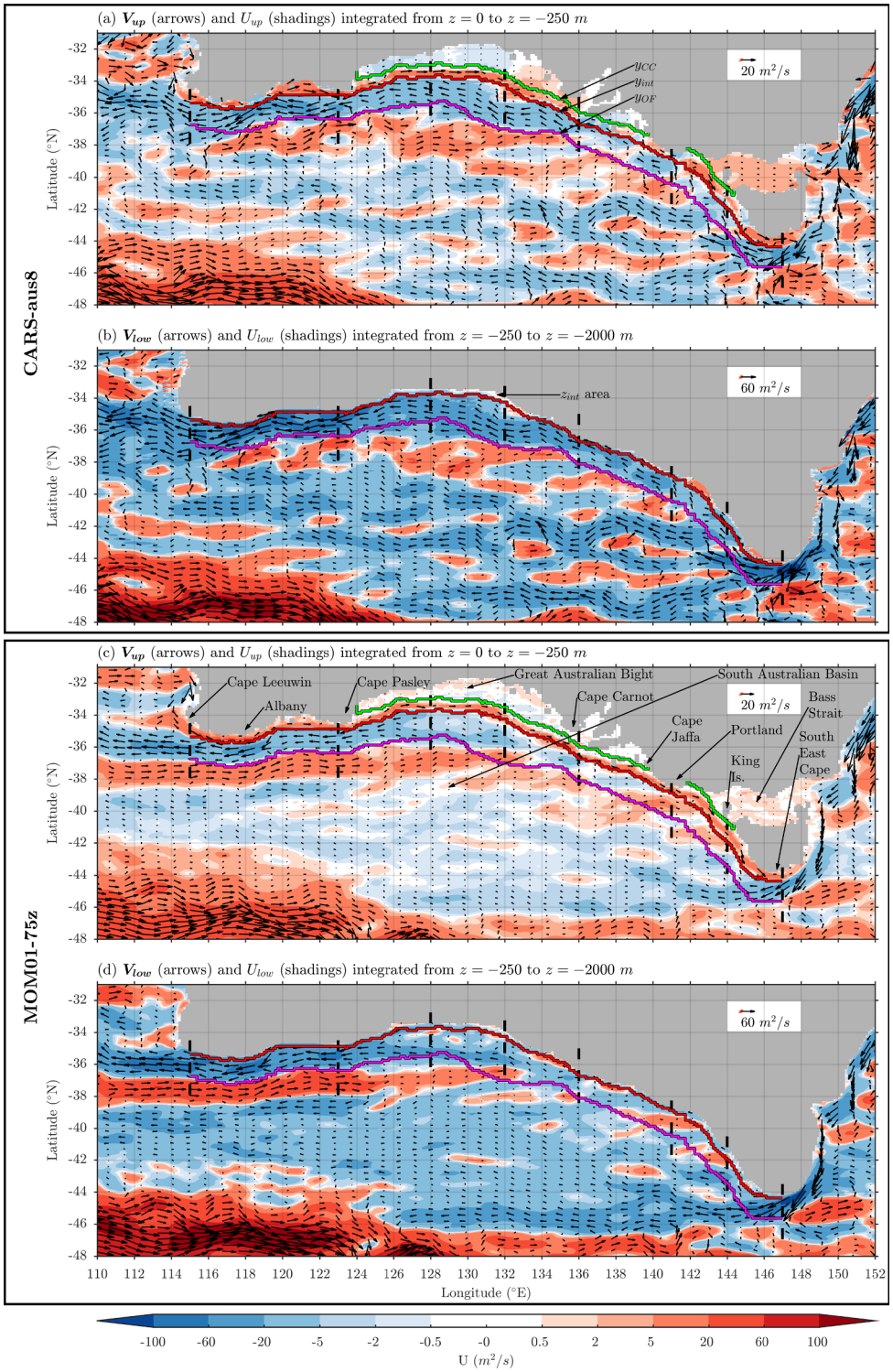

Fig. 3. Depth integrated (a,b) geostrophic velocities in CARS and (c,d) full velocities in MOM01, showing the velocity field (directional plot) and the zonal component (shadings, non-monotonic scale) in $m^2 s^{-1}$ (ie. transport per unit width). The fields are integrated from (a,c) the surface to −250 m and from (b,d) −250 m to −2000 m. In CARS, (a) shows the sum of geostrophic velocities and Ekman velocities and (b) shows geostrophic velocities only. Boundaries of the SBC and FC as follows: y_{CC} (green with black outline) is the SBC north boundary; y_{int} (red with black outline) is the SBC south boundary and the FC north boundary; y_{OF} (magenta with black outline) is the FC south boundary; z_{int} area is the surface bounded by y_{int} at south and the slope at north. (For interpretation of the references to colour in this figure legend, the reader is referred to the web version of this article.)

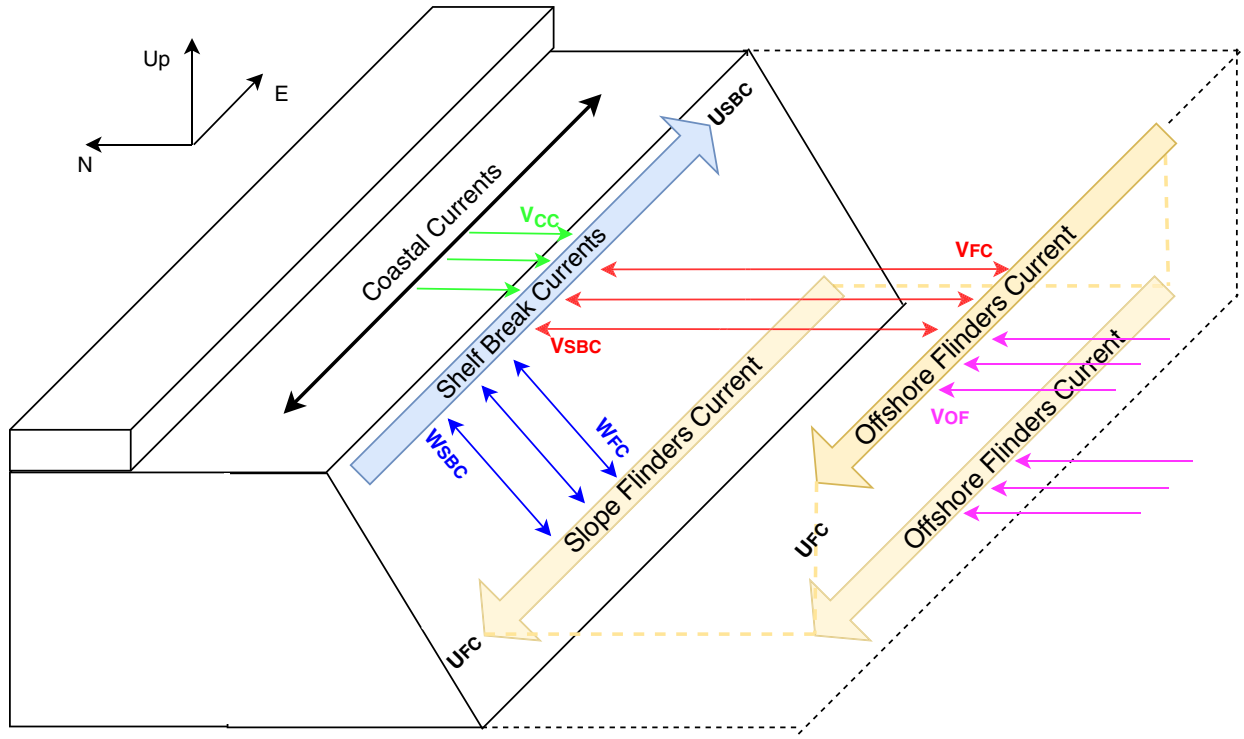

Fig. 4. Southern Australia Current System transport budget schematic. The SBC transport is shown as a thick light blue arrow, the offshore-FC and slope-FC transports as thick light yellow arrows. The shallow coastal currents are shown as a black two-ways arrow. The inward/outward transports into/out of the SBC and FC are shown as thin coloured arrows. The budget includes four transport exchanges: horizontal exchange between coastal currents and SBC (green arrows), horizontal exchange between SBC and upper offshore-FC (red arrows), vertical exchange between SBC and slope-FC (blue arrows) and horizontal exchange between ocean interior onshore flows and offshore-FC (magenta arrows). (For interpretation of the references to colour in this figure legend, the reader is referred to the web version of this article.)

(Fig. 3). Here the boundary colours match up with transport exchange vectors in Fig. 4. Note there is no vertical flow across the FC bottom as this boundary is at the reference depth z_{ref} (Fig. 2, cyan line). Details of SBC and FC lateral boundary definitions are set out in Appendix B.

2.4. Transport budget derivation

We calculate the local zonal transport within the SBC and FC volumes, which we refer to as SBC and FC transport. The in/outward transport across volume boundaries (including geostrophic and Ekman) is referred to as cross-boundary transport. As a reminder, in CARS, the SBC transport includes geostrophic flow and Ekman drift. The FC transport includes geostrophic flow and Ekman drift in the upper layer, and geostrophic flow only in the lower layer. In MOM01, we carry out the same calculations and also estimate transports from full velocity. Below, we provide identities for SBC and FC transport that include cross-boundary exchanges. The following equations represent a transport in volume per unit time in Sverdrups (Sv, 10^6 m^{3}s^{-1}).

We choose to use Cartesian coordinates, rather than coast-following, because the currents are narrow and it is difficult to define a coast-following coordinate system that conserves mass in the transport calculations. Our approach ensures mass conservation through careful selection of grid cells in the transport budget, and capturing of all flow into and out of each cell, as explained in Appendix C.

The following transport equations are indicated in Fig. 4. The SBC transport $\mathscr{U}_{\text{SBC}}$ is

$$\mathscr{U}_{\text{SBC}}(x) = \int_{y_{\text{int}}(x)}^{y_{\text{CC}}(x)} U_{\text{up}}\, dy, \tag{3}$$

where y_{int} is the SBC southern boundary (Fig. 3a), y_{CC} is the SBC northern boundary (Fig. 3a), and U_{up} is the zonal component of velocity in (1). Hence $\mathscr{U}_{\text{SBC}}$ represents the upper layer zonal transport bounded by y_{int} and , where positive means an eastward SBC transport.

The cross-boundary transport from coastal currents and from the offshore-FC into the SBC are

$$\mathscr{V}_{\text{CC}}(x) = \int_{x_{\text{west}}}^{x} \mathbf{n}_{\text{CC}}\cdot\mathbf{V}_{\text{up}}\, dl_{\text{CC}}, \tag{4}$$

$$\mathscr{V}_{\text{SBC}}(x) = \int_{x_{\text{west}}}^{x} \mathbf{n}_{\text{int}}\cdot\mathbf{V}_{\text{up}}\, dl_{\text{int}}, \tag{5}$$

where $x_{\text{west}} = 115^{\circ}$E is the SBC western edge longitude, dl_{CC} and dl_{int} are the line elements of the curves y_{CC} and y_{int}, respectively, from x_{west} to x, and $\mathbf{n}$ is a unit vector perpendicular to dl and pointing into the SBC. $\mathscr{V}_{\text{CC}}$ and $\mathscr{V}_{\text{SBC}}$ hence represent the horizontal cross-boundary transport, accumulated from x_{west} to x, across y_{CC} (positive from the coastal currents into the SBC) and across y_{int} (positive from offshore-FC into the SBC), respectively. Here, since the transport is accumulated from west to east, positive means a net inflow into the SBC.

The vertical transport from the slope-FC into the SBC is defined as

$$\mathscr{W}_{\text{SBC}}(x) = \int_{x_{\text{west}}}^{x} \int_{y_{\text{int}}(x)}^{y_{\text{CC}}(x)} \nabla\cdot\mathbf{V}_{\text{up}}\, dy\, dx. \tag{6}$$

where y_{int} is the SBC bottom boundary (Fig. 2c). Hence $\mathscr{W}_{\text{SBC}}$ represents the transport across the depth-level z_{int} (from the slope-FC into the SBC), accumulated from x_{west} to x. Positive $\mathscr{W}_{\text{SBC}}$ means a net upwelling flow into the SBC.

The FC transport $\mathscr{U}_{\text{FC}}$ is

$$\mathscr{U}_{\text{FC}}(x) = \int_{y_{\text{OF}}(x)}^{y_{\text{ini}}(x)} U_{\text{up}}\, dy + \int_{y_{\text{OF}}(x)}^{y_{\text{slope}}(x)} U_{\text{low}}\, dy, \tag{7}$$

where y_{OF} is the FC southern boundary (Fig. 3a), y_{slope} is the slope (northern) boundary at z_{int}, and U_{low} is the zonal component of velocity in (2). Hence $\mathscr{U}_{\text{FC}}$ represents the zonal transport bounded by y_{OF} and y_{int} in the upper layer (i.e. the near-surface offshore-FC) and bounded by

y_{OF} and the slope in the lower layer (i.e. the slope-FC and the deep offshore-FC); where positive means an eastward FC transport.

The cross-boundary transport from South Australian Basin onshore flows, representing inputs from the ocean interior, is defined as

$$\mathscr{V}_{OF}(x) = \int_{x}^{x_{east}} \mathbf{n}_{OF}\cdot(\mathbf{V}_{up} + \mathbf{V}_{low})\, dl_{OF}, \tag{8}$$

where $x_{east} = 147°E$ is the FC eastern edge, dl_{OF} is the line element of y_{OF} from x to x_{east} and $\mathbf{n}$ is a unit vector perpendicular to dl and pointing into the FC. $\mathscr{V}_{OF}$ thus represents the horizontal transport across the boundary y_{OF} and into the FC, accumulated from x to x_{east}. Since this transport is accumulated from west to east, positive is a net input from onshore flows into the FC.

The other cross-boundary transports into the FC across y_{int} and z_{int} are equal and opposite to the corresponding SBC cross-boundary transports (ie. $\mathscr{V}_{SBC}$ and $\mathscr{W}_{SBC}$, respectively). Hence

$$\mathscr{V}_{FC}(x) = \int_{x}^{x_{east}} -\mathbf{n}_{int}\cdot\mathbf{V}_{up}\, dl_{int}, \tag{9}$$

$$\mathscr{W}_{FC}(x) = \int_{x}^{x_{east}} \int_{y_{int}(x)}^{y_{CC}(x)} -\nabla\cdot\mathbf{V}_{up}\, dy\, dx, \tag{10}$$

where $\mathscr{V}_{FC}$ and $\mathscr{W}_{FC}$ represent the cross-boundary transports, accumulated from x to x_{east}, across y_{int} (positive is a net horizontal SBC input) and across z_{int} (positive is a net downwelling input from the SBC), respectively.

Finally, since the geostrophic and Ekman velocities (readjusted via the Zero-divergence method, Appendix A.2) and MOM01 full velocities are mass conserving, the SBC transport $\mathscr{U}_{SBC}$ and FC transport $\mathscr{U}_{FC}$ can also be obtained from the Continuity equation by interpreting the cumulative transport terms (i.e. the cross-boundary transports) as sources and sinks. Hence,

$$\mathscr{U}_{SBC}(x) = \mathscr{U}_{SBC}(x_{west}) + \mathscr{V}_{CC}(x) + \mathscr{V}_{SBC}(x) + \mathscr{W}_{SBC}(x). \tag{11}$$

$$-\mathscr{U}_{FC}(x) = -\mathscr{U}_{FC}(x_{east}) + \mathscr{V}_{FC}(x) + \mathscr{V}_{OF}(x) + \mathscr{W}_{FC}(x). \tag{12}$$

Note that in Eq. 12, there is a negative sign in front of $\mathscr{U}_{FC}(x)$ because the FC transport is westward, that is in the negative direction, therefore its sign is changed so that inputs into the current (i.e. positive cross-boundary flows) are translated into a stronger FC. We calculate all transport terms using definitions 3–10 and verify that the above equalities are satisfied at very high accuracy. This test is shown in Appendix C.1.

3. Results

This section is divided into three subsections. Firstly, we describe the Southern Australia Current System annual-mean, three-dimensional structure (Section 3.1). Secondly, we analyse the system transport budget (Section 3.2). Finally, we discuss the annual-mean SBC–FC coupling and present an overview of the summer and autumn states (Section 3.3).

3.1. Southern Australia Current System Structure

Here, we identify the main current features in velocity sections (Section 3.1.1) and in depth integrated velocity maps (Section 3.1.2). In these two subsections we provide enhanced confidence in our findings by comparing the observation-based product CARS with the model data from MOM01. Finally, we examine vertical flows over the shelf in MOM01 (Section 3.1.3).

3.1.1. Shelf meridional sections

From Cape Leeuwin to Cape Pasley (the two westernmost sections, Fig. 2a,b,i,j), the Leeuwin Current Extension weakens in both CARS and MOM01. Estimates from Cresswell and Griffin (2004) and Cresswell and Peterson (1993) also show a stronger Leeuwin Current Extension and more intense eddies near Cape Leeuwin. From the western Great Australian Bight through to King Island (Fig. 2c-g,k-o), the South Australian Current and the Zeehan Current are generally weaker. MOM01 helps identify the current structure in some sections where it is not represented in CARS (e.g. Cape Carnot and Portland sections). Not much is known on the South Australian Current, apart from it being weaker than the Leeuwin Current Extension (Middleton and Bye, 2007) and that it is altered by coastal runoff from the Bight (Rochford, 1986). Off South East Cape (easternmost section, Fig. 2h,p), the Zeehan Current intensifies, which is consistent with Oliver and Herzfeld (2016, 2018) who found a strong current there continuing over the eastern Tasmanian shelf. Overall, the SBC are strongest at the western and eastern ends of the domain (Cape Leeuwin and South East Cape) where they reach mean speeds up to 20 cm s^{-1}.

Since the hydrographic observations fed into CARS are spatially and temporally non-uniform (see Ridgway et al., 2002 discussion in Section 2.1), a CARS versus MOM01 comparison is essential to ensure the current structure and speed represented in CARS is robust. Here, the general agreement between CARS and MOM01 suggests that the topography-adapted interpolation method applied in CARS is suitable to analyse narrow boundary currents at high-resolution. This agreement is impressive given that Argo data cannot contribute to the hydrographic observations over the shallow shelf.

We next identify the FC found offshore and underneath the SBC. Offshore South East Cape, we consider the strong, deep-reaching westward flow to be the Tasman Leakage, following Speich et al.'s (2002, 2012, 2014) description. We discuss the discontinuity between the Tasman Leakage and FC later, when we analyse velocity maps. Here, we analyse the flow distinction between the slope-FC and offshore-FC along the slanted and zonal shelves.

The slope-FC is located around 600 m and found in most sections along the slanted shelf (from Cape Carnot to King Island) and the zonal shelf (from Cape Leeuwin to western Bight). The slope-FC also intensifies to the west towards Cape Leeuwin. Generally, the CARS and MOM01 slope-FC agrees well with Middleton and Bye's (2007) velocity records (3–7 cm s^{-1}) and depth range estimates (500–1000 m). At the eastern Bight, the only section with a gentle slope, the slope-FC is absent in CARS and weakest in MOM01. This suggests that a zonal shelf and a steep slope may play a role in maintaining a strong slope-FC.

The offshore-FC also intensifies to the west towards Cape Leeuwin. The offshore-FC is either weaker or detached from the slope-FC where the shelf slant is strong (Portland and King island sections) and where the slope is gentle (eastern Bight section). While the shelf orientation and slope steepness may play a role in maintaining these FC components, the detachment between the slope-FC and the offshore-FC may indicate they are independent features occasionally merging and separating as the topography varies. Overall, the FC is strongest at Cape Pasley and Cape Leeuwin where it reaches mean speeds up to 10 cm s^{-1}, which agrees well with FC speed records from Cresswell and Peterson (1993).

One noticeable difference between CARS and MOM01 is at the Cape Leeuwin section. In CARS, the FC weakens and splits producing another westward flow further offshore. In MOM01, this further offshore flow is eastward. In the next sub-Section, we identify this vertically coherent eastward jet as the southern arm of the anti-cyclonic Albany High (Middleton and Platov, 2003; Middleton and Bye, 2007; McCartney and Donohue, 2007) clearly visible off Cape Leeuwin and Cape Pasley in MOM01.

3.1.2. Depth-integrated velocity maps

We now examine the upper and lower layer velocity fields in depth-integrated velocity maps (Fig. 3). In CARS, the SBC eastward flow is interrupted by reversals, notably near Albany, between Cape Carnot and Cape Jaffa, and west of Tasmania (Fig. 3a). Localised SBC reversals there may due to the mean field capturing some of the intense eddy activity over the shelf, which was also observed in MOM01 on 5-day average timescales (not shown). They may also be due to

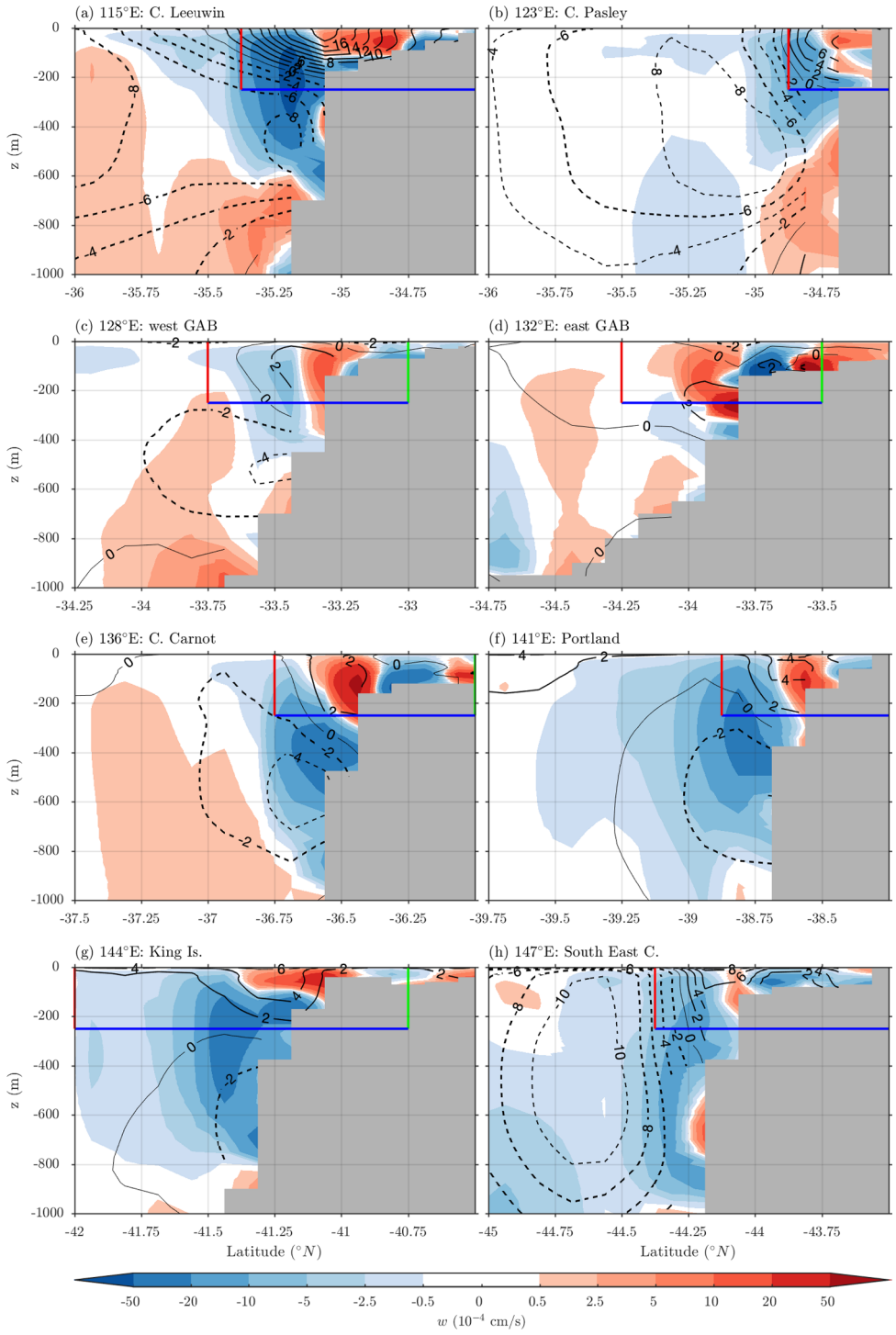

Fig. 5. Meridional sections along southern Australia of vertical and zonal full velocities in MOM01, zoomed over the shelf break region. Vertical velocities w in 10^{-4} cm s^{-1} (shadings) and zonal velocities u in cm s^{-1} (contours, every 2 cm s^{-1}, thick solid lines show positive values, thick dashed lines show negative values, thin solid lines show zero contour). Boundaries of the SBC as follows: y_{CC} (green) is the SBC north boundary; z_{int} (blue) is the SBC bottom boundary and the FC top boundary; y_{int} (red) is the SBC south boundary and the FC north boundary. (For interpretation of the references to colour in this figure legend, the reader is referred to the web version of this article.)

undersampling in CARS as described in Section 2.1. Regardless, the SBC magnitude and width agree well between CARS and MOM01. In MOM01, the SBC flow is a narrow, continuous eastward boundary current (Fig. 3c).

The narrow slope-FC is not discernible as a distinct current in this depth-integrated view, so we next analyse wide horizontal structure of the offshore-FC. Along the slanted shelf and in the upper layer, the FC is weak and locally reversed in CARS and MOM01. In the lower layer, the FC is continuous in CARS (Fig. 3c) and more coherent in MOM01 (Fig. 3d), perhaps because the deep flow is less affected by surface intensified mesoscale structures. Along the zonal shelf, the FC firmly emerges as a wide, westward-intensifying, westward flow in both layers.

Further offshore, the long-term average field tends to reveal

mesoscale structures in CARS and laminar flows in MOM01. For example, in CARS, the eastward jet south of the FC is vertically coherent but horizontally patchy, and absent off Cape Leeuwin, due to the FC offshore spreading found earlier (Fig. 2a). In MOM01, the eastward jet is coherent horizontally and vertically, at least until the Great Australian Bight. At South East Cape, the Tasman Leakage outflows via westward-flowing meandering structures in CARS, whereas it outflows mostly due westward in MOM01. In both layers and datasets, the Tasman Leakage flows away from the western Tasmanian shelf; it is unclear from these velocity fields whether any Tasman Leakage flow is carried into the FC. The transport budget in Section 3.2 provides insights into the Tasman Leakage-to-FC connection.

3.1.3. Vertical flows in MOM01

This section briefly examines vertical flows between the SBC and slope-FC. Fig. 5 shows meridional sections of vertical and zonal velocity components from MOM01, zoomed into the shelf break and the upper slope. This time, blue-red shadings illustrate vertical flows and contours show zonal velocities.

Our sections show strong downwelling flows near the shelf break and upper slope. These flows are located approximately on the seaward side and lower portion of the SBC. They are strong between 100 and 600 m and generally intrude into most of the slope-FC (Fig. 5a,e,f,g). The Leeuwin Current Extension exhibits a strong downwelling into the slope-FC at Cape Leeuwin (Fig. 5a) with speeds greater than -50×10^{-4} cm s^{-1}. In the eastern Bight section (Fig. 5d), where the upper slope is gentle and the slope-FC is absent, an upwelling flow dominates at the South Australian Current bottom boundary. In the subsequent slanted shelf sections at Cape Carnot, Portland and King island (Fig. 5e,f,g) downwelling is greater than -20×10^{-4} cm s^{-1} and generally stronger than that along the zonal shelf sections (Fig. 5b,c,d, Cape Leeuwin section excluded). Off South East Cape (Fig. 5h), downwelling dominates the upper 1000 m and flows through the onshore portion of the Tasman Leakage.

The slope-FC co-exists with the SBC downwelling coming from above. At the only section where the slope-FC is absent (off the eastern Great Australian Bight Fig. 5d), the vertical flow is upwelling. This suggests that downwelling is important to maintain the slope-FC. Within the lower portion of the FC, a deep upwelling generally exists along the zonal shelf sections and at Cape Carnot (Fig. 5a–e). In the remaining slanted sections, a weak upwelling exists deeper than 1000 m (not shown) while the layer above it is dominated by SBC downwelling. This configuration consisting of a downwelling shelf break current and an upwelling counter-flowing undercurrent (slope current) was also described in Woo and Pattiaratchi's (2008) analysis of the Leeuwin Current System along western Australia who also conjectured that the SBC–slope-FC pair essentially has the same structure as the Leeuwin Current–Leeuwin Undercurrent pair.

To summarise, downwelling flows exist in the lower and seaward portion of the SBC and intrude into the slope-FC. The downwelling flows cover most of the slope-FC, but in one section off the eastern Great Australian Bight section, the slope is gentler, the slope-FC is absent, and the vertical flows at the SBC bottom are upwelling. This suggests that both the downwelling and the slope-FC exist where the continental slope is steep. The downwelling is strong at Cape Leeuwin (greater than -50×10^{-4} cm s^{-1}) and extends deeper off the slanted shelf sections (speed greater than -20×10^{-4} cm s^{-1}) and off South East Cape where they dominate the upper 1000 m.

3.2. Southern Australia Current System Transport Budget

The CARS and MOM01 long-term mean transport budget (Fig. 6) as derived from the equations in Section 2.4 is analysed for the SBC (Section 3.2.1) and the FC (Section 3.2.2). This budget describes the along-shore evolution of the transports $\mathscr{U}_{SBC}$ (Eq. (3)) and $\mathscr{U}_{FC}$ (Eq. (7)). It also quantifies horizontal and vertical flows into and out of the SBC which are referenced in Fig. 6 ($\mathscr{V}_{CC}$, Eq. (4); $\mathscr{V}_{SBC}$, Eq. (5); $\mathscr{W}_{SBC}$, Eq. (6)) and the FC ($\mathscr{V}_{OF}$, Eq. (8); $\mathscr{V}_{FC}$, Eq. (9); $\mathscr{W}_{FC}$, Eq. (10)). This analysis is further summarised and simplified in Section 4 and Fig. 10.

3.2.1. SBC budget

The SBC transport $\mathscr{U}_{SBC}$ (Eq. (3), Fig. 6a black lines) exhibits significantly higher variations in CARS than in MOM01, particularly in the Leeuwin Current Extension (see also Fig. 3, see Section 3.1 for CARS versus MOM01 discussion). Nonetheless, the trend of the South Australian Current and the Zeehan Current transport in CARS roughly agrees with those in MOM01. Because transport variability is stronger in CARS, we describe the transport evolution and changes from full transport in MOM01, simply because it is easier to identify them in MOM01. It is worth noting here that in MOM01, the transport adjusted via the Zero Divergence method (i.e., Ekman plus geostrophic transport from the Zero Divergence method applied to the model's temperature and salinity field and wind data) agrees very well with the full transport determined from the model's full velocity field.

From west to east, the Leeuwin Current Extension decreases from $\mathscr{U}_{SBC} = 1.1$ to about 0.1 Sv, the South Australian Current fluctuates with the transport across the zonal shelf remaining stable and that across the slanted shelf increasing to 0.3 Sv, and the Zeehan Current slightly increases to about 0.4 Sv. The Leeuwin Current Extension decrease from west to east is consistent with Yit Sen Bull and van Sebille's (2016) transport budget although their Lagrangian current transport estimates were stronger. One explanation is our fixed boundary transport budget can, in some places, include westward flows from the adjacent FC, possibly underestimating our Leeuwin Current Extension transport. The difference may also be due to the choice of transport weighting for particles in their experiment.

The cumulative cross-boundary transport between the coastal current and SBC $\mathscr{V}_{CC}$ (Eq. (4), Fig. 6a green lines) are weak in the Great Australian Bight and Gulf regions with a net exchange up to $\mathscr{V}_{CC} = +0.1$ Sv. Over Bass Strait, there is a net outflow from the SBC of 0.2 Sv. The cumulative cross-boundary transport between the SBC and the FC are presented in Fig. 6b. On average, the Leeuwin Current Extension loses water horizontally to the FC as the cumulative horizontal transport ($\mathscr{V}_{SBC}$, Eq. (5), Fig. 6b red lines) is negative in the entire Leeuwin Current Extension region. Specifically, the Leeuwin Current Extension loses $\mathscr{V}_{SBC} = -0.5$ Sv up to 119°E near Albany, which indicates that the Leeuwin Current partly outflows horizontally into the offshore-FC as it turns around the south-west corner of Australia to become the Leeuwin Current Extension. East of Albany, the opposite happens where the upper offshore-FC generally feeds horizontally into the SBC. The total horizontal inflow into the SBC from Cape Leeuwin to South East Cape is +1.5 Sv.

The model vertical exchanges between the SBC and the FC ($\mathscr{W}_{SBC}$, Eq. (6), Fig. 6b blue lines) reveal a persistent downwelling out of the SBC that increases steadily from west to east. To this downwelling, the Leeuwin Current Extension contributes $\mathscr{W}_{SBC} = -0.8$ Sv, the South Australian Current −0.7 Sv and the Zeehan Current −0.5 Sv. This provides a total downwelling of −2 Sv out of the SBC between Cape Leeuwin and South East Cape (Fig. 10). Eighty percent of the decrease in the Leeuwin Current Extension's transport from $\mathscr{U}_{SBC} = 1.1$ to 0.1 Sv is due to the downwelling. The zonal South Australian Current's steady transport is maintained by compensating lateral inflows that balance the downwelling in this region. The weak increase in the slanted South Australian Current's transport and the Zeehan Current's transport is essentially due to an increase in lateral inflows.

To summarise, as the Leeuwin Current Extension flows around the southwest corner of Australia, it loses most of its transport due to downwelling and lateral offshore flow. Then the downwelling is reduced and the western South Australian Current flows along the zonal shelf break without much systematic change in its transport. As the South Australian Current flows over the slanted shelf break, it receives progressively increasing lateral inflows which are partly overturned by

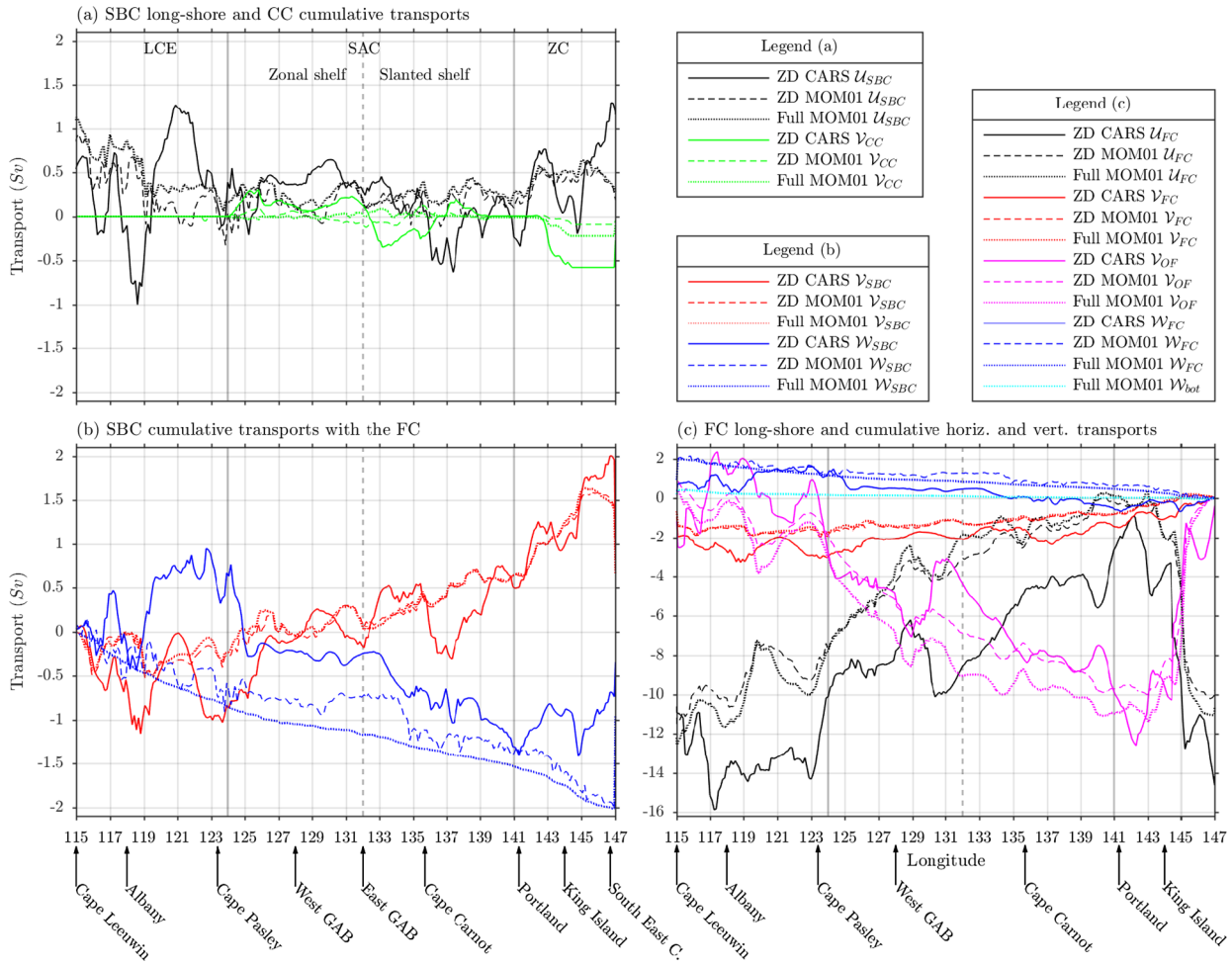

Fig. 6. Southern Australia Current System transport budget (*Sv*) for (a) the SBC transport (black, positive eastward) and the horizontal cumulative (west to east) cross-boundary transport along y_{CC} (green, positive into the SBC), (b) the SBC cumulative (west to east) cross-boundary transport exchanged with the FC horizontally across y_{int} (red, positive into the SBC) and vertically across z_{int} (blue, positive into the SBC), (c) the FC transport (black, positive eastward), cumulative (east to west) cross-boundary transports with the SBC (red and blue, positive into the FC), and cumulative (east to west) cross-boundary horizontal transport along y_{OF} (magenta, positive into the FC). Results are shown for the "Zero Divergence" (ZD, Furue et al., 2017) adjusted transports in the observations (solid lines) and in the model (dashed lines), and also the actual model transports (thin dotted line). The thin dotted cyan line shows the actual model vertical transport at the bottom of the FC (this is absent in the geostrophic transport). The vertical solid gray lines separate the Leeuwin Current Extension, South Australian Current and Zeehan Current and the vertical dashed grey line separates the region with a zonal shelf to the west from the region with a slanted shelf to the east. (For interpretation of the references to colour in this figure legend, the reader is referred to the web version of this article.)

weakly increasing downwelling flows, resulting in a stronger slanted South Australian Current. The Zeehan Current grows in a similar way, where the lateral inflow is strong enough to overcome the losses to the downwelling and a lateral outflow into Bass Strait. Overall, the SBC transport decrease from $\mathscr{U}_{SBC} = 1.1$ Sv at Cape Leeuwin to 0.4 Sv at South East Cape is due to a $\mathscr{V}_{SBC} = +1.5$ Sv; lateral inflow from the FC minus a $\mathscr{W}_{SBC} = -2$ Sv downwelling back into the FC and a weak lateral $\mathscr{V}_{CC} = -0.2$ Sv shallow loss into Bass Strait.

3.2.2. FC budget

The FC and cross-boundary cumulative transports are presented in Fig. 6c. The transport $\mathscr{U}_{FC}$ (Eq. (7), Fig. 6c black lines) displays large variations in CARS as for the SBC. Here the FC is generally stronger in CARS than in MOM01, with a westward transport in the observations up to 6 Sv stronger. Both in CARS and MOM01, the transport undergoes a sudden loss in westward transport because of the Tasman Leakage (see also Fig. 3). The loss varies from $\mathscr{U}_{FC} = -11$ Sv at South East Cape to around zero near Portland (a negative transport is westward). The fact that the FC transport goes to zero past the Tasman Leakage suggests that the Tasman Leakage flow does not enter the FC. A Tasman Leakage retroflection northward along the western Tasmanian shelf is not obvious in our transport budget, which is consistent with Speich et al.'s (2002, 2012, 2014) description of a lack of Tasman Leakage-to-FC connection. The FC intensifies along the slanted coast to reach −1.8 Sv at the eastern Great Australian Bight; and along the zonal coast to reach −7.7 Sv at Cape Pasley and −12.3 Sv at Cape Leeuwin. In contrast to the SBC, the FC thus intensifies monotonically as it flows westward.

The exchanges between the FC and the SBC are relatively insignificant in determining this increase in the FC transport as the main contributors to the FC strengthening are the onshore flows across the FC's southern boundary (Eq. (8)). The spatial structure of the change in $\mathscr{U}_{FC}$ therefore mirrors that of $\mathscr{V}_{OF}$ (Fig. 6c). Overall, the FC transport increases from near zero (after the Tasman Leakage leaves the coast) to $\mathscr{U}_{FC} = -12.3$ Sv at Cape Leeuwin due to a net + 11.8 Sv gain from the onshore flows. Out of this net inflow, 20.3% occurs along the slanted shelf (+2.4 Sv), 50% in the zonal Great Australian Bight region (+5.9 Sv) and 29.7% in the zonal shelf region from Cape Carnot to Cape Leeuwin (+3.5 Sv). Nearly 80% of the onshore flow contribution to the FC increase occurs along the zonal shelf.

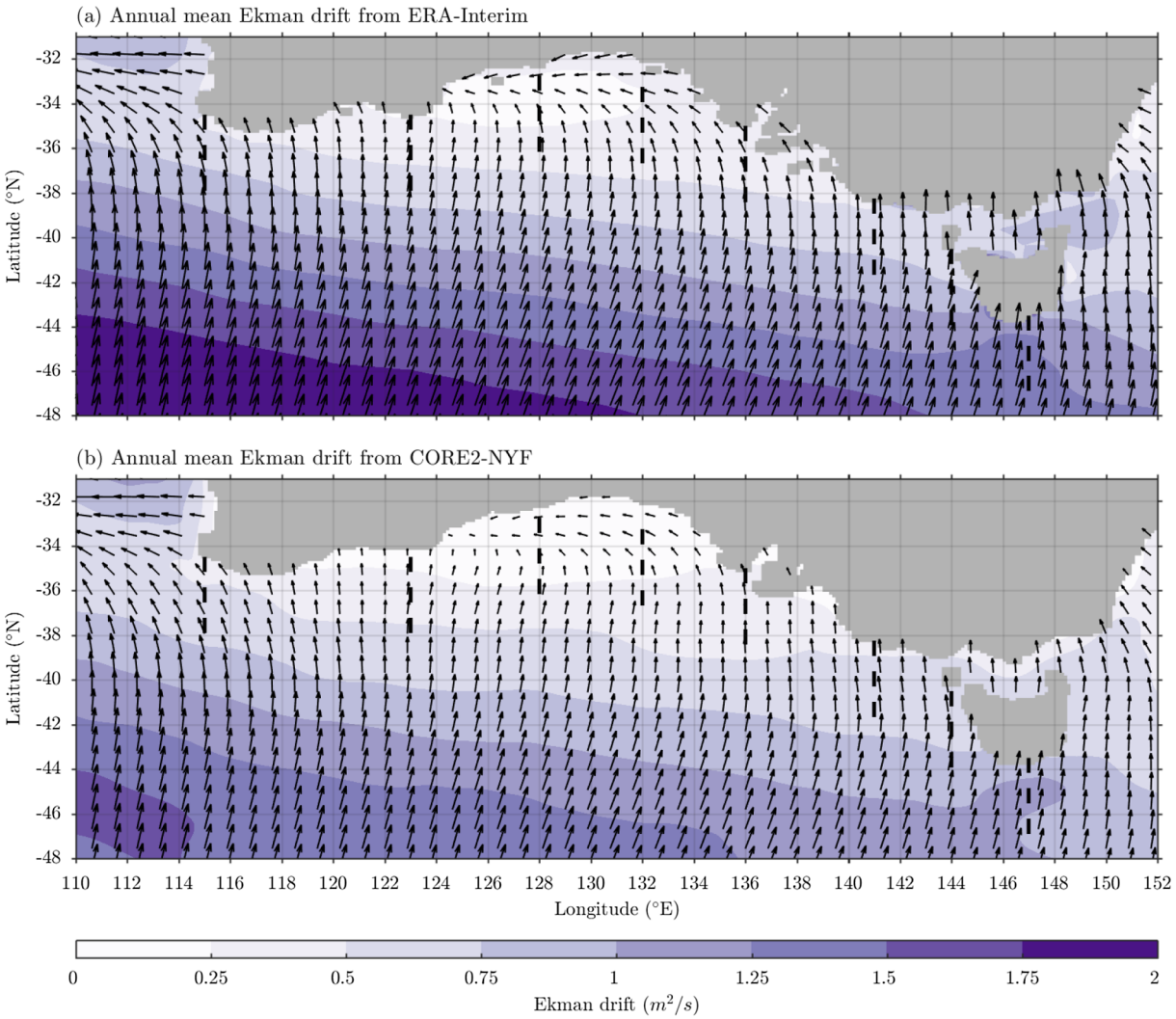

Fig. 7. Long-term mean Ekman drift ($m^2\,s^{-1}$) estimated from (a) ERA-Interim winds and (b) CORE2-NYF winds (see Section 2.1). The magnitude of the Ekman drift is indicated by the shading. To illustrate weaker flows better, arrow lengths are proportional to the square root of the vector amplitudes.

3.3. SBC and FC coupling

The Southern Australian Current System transport budget revealed that a large part of the onshore flow into the FC is directly converted into increasing westward transport from close to zero along western Tasmania to 12.3 Sv near the western side of Australia.

Further inshore, there is a coupling between the SBC and offshore-FC which provides a lateral source water for the SBC. We examine maps of Ekman drift in Fig. 7 to provide a mechanism for such lateral inflow into the SBC. We find that the annual-mean Ekman drift in ERA-Interim (which was used with the CARS geostrophic velocities to calculate the transport in CARS, Fig. 7a) is slightly stronger than the Ekman drift in CORE2-NYF (which was used to force MOM01, Fig. 7b). The Ekman drift is generally pointing northward, hence onshore everywhere except in the Great Australian Bight and southeast in front of the Gulfs where it decreases and turns westward. The onshore Ekman drift provides a coupling mechanism between the offshore-FC and SBC, explaining the lateral inflow from the offshore-FC into the SBC.

The transport budget also revealed a coupling between the SBC and the slope-FC where the Ekman drift is downwelled into the slope-FC. We examine maps of vertical flows at the depth z_{int} in MOM01 (Fig. 8)) to examine the spatial variability of the annual-mean vertical motion along the coast. We note that we do not show the vertical velocities produced by the Zero-Divergence adjustment, neither in this Figure nor in Fig. 5. This is because the geostrophic calculation (before and after the Zero-Divergence adjustment) produces a noisy vertical-velocity field above complex bottom topography (evident in Fig. 6b,c in local reversals of accumulated upwellings/downwellings). Thus, these fields are useful only when integrated over a long distance as in our cumulative transport calculations. For example, the longshore integration of vertical velocities at the SBC base (Eq. 6) reveals the vertical velocity that compensates the SBC flow above it.

The vertical flows along the upper slope at -250 m are downwelling throughout the southern Australian shelves. The downwelling is strong where the slope is steep, particularly outside the Great Australian Bight region. In the Bight, the slope is less steep and the downwelling is weaker. The primarily onshore direction of the Ekman drift is consistent with the downwelling found all along the coast. The downwelling is most pronounced in the Leeuwin Current Extension and Zeehan Current regions, where the onshore Ekman drift is strongest (Fig. 7). In the Bight and Gulf regions the Ekman drift curls anticlockwise resulting in weak downwelling, which is further reduced in the Bight where the slope is less steep.

Finally, there is also an inverse seasonal relationship between the SBC and the FC which we briefly discuss here. Fig. 9 shows the summer and autumn states in MOM01 for the SBC transport ($\mathscr{U}_{\text{SBC}}$, Fig. 9) and the FC transport ($\mathscr{U}_{\text{FC}}$, Fig. 9b). We show all seasons but analyse only the summer and autumn states as they exhibit the strongest deviation

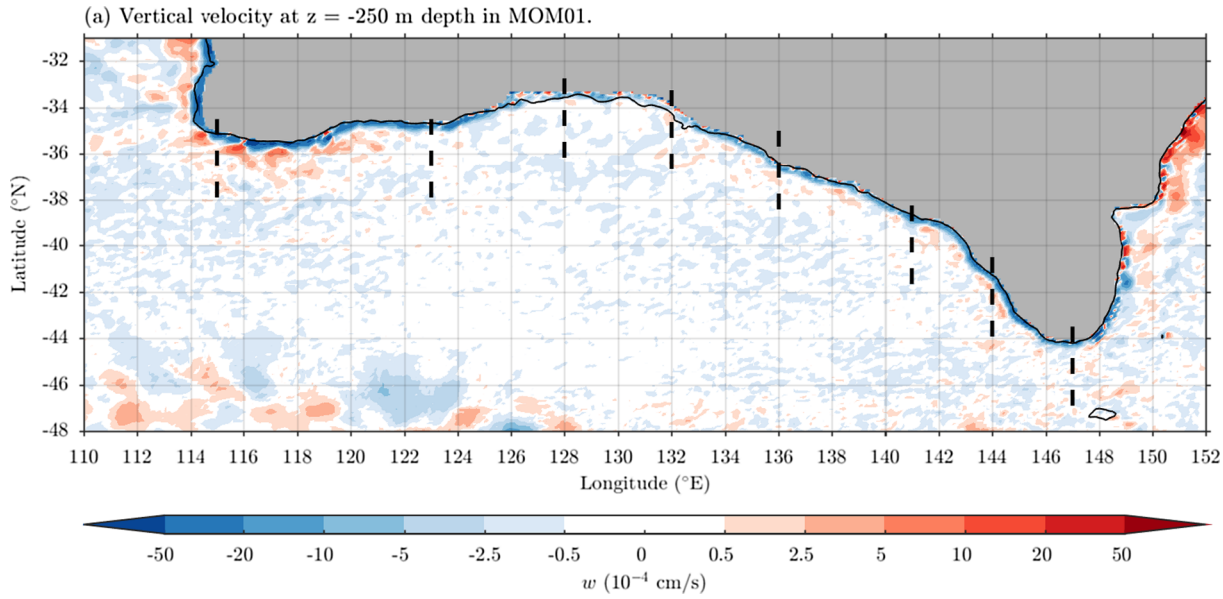

Fig. 8. Long-term mean full model vertical velocity field at $z_{int} = -250$ m in 10^{-4} cm s^{-1} (with nonlinear shading levels) in MOM01. The thin black line shows the 1000 m isobath. The grey region is where $z > -250$ m.

from the annual-mean. Oke et al. (2018) also found that the SBC are strongest in autumn, decrease in winter and spring and are weakest in summer.

In summer, the SBC are weakest and reversed in many places along the coast, particularly in the zonal South Australian Current region (Fig. 9a). On average, the Leeuwin Current Extension, the slanted South Australian Current and the Zeehan Current carry very little eastward transport, and the zonal South Australian Current is strongly westward at 0.6 Sv on average with a maximum westward transport reaching 1 Sv. The zonal South Australian Current exhibits the largest seasonal changes in transport. In summer, the weak SBC can be explained by the mostly offshore direction of the Ekman drift along the coast,

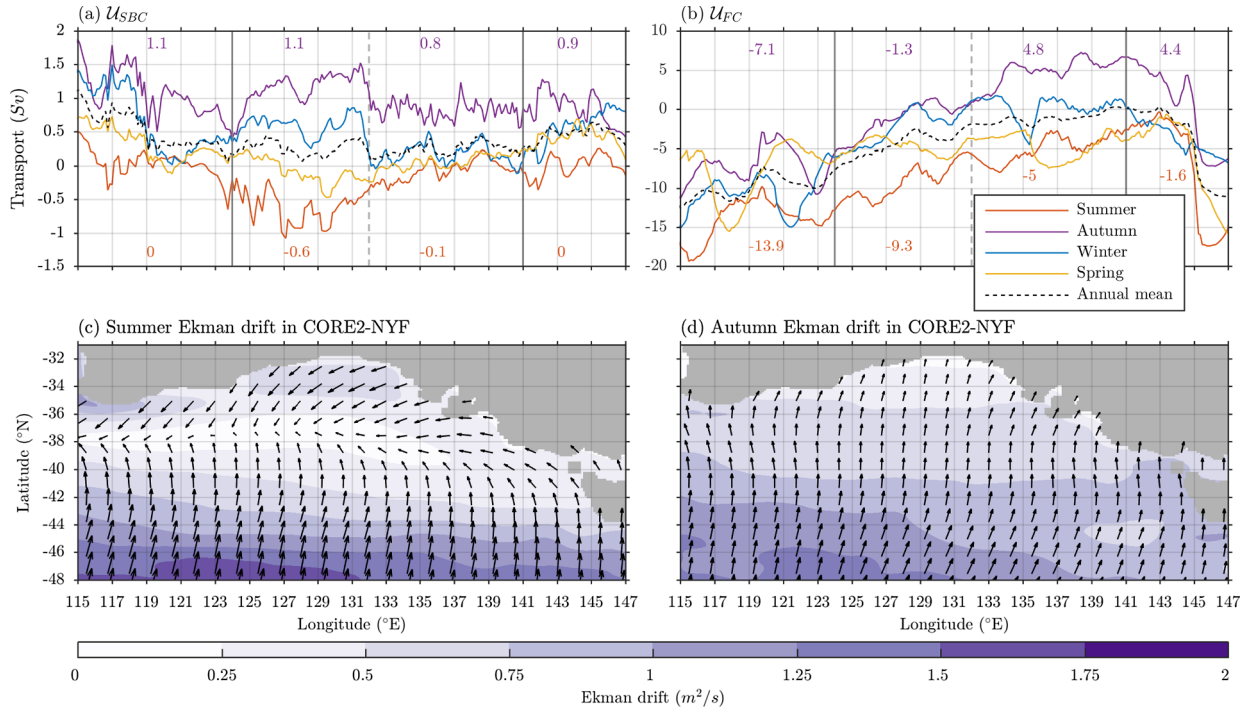

Fig. 9. Summer mean (orange lines), autumn mean (purple lines), winter mean (blue lines), spring mean (yellow lines) and annual-mean (black dashed lines) in MOM01 for (a) the SBC transport ($\mathcal{U}_{SBC}$, positive eastward) and (b) the FC transport ($\mathcal{U}_{FC}$, positive eastward); and Ekman drift derived from CORE2-NYF winds in (c) summer and (d) autumn. In (a) and (b), the vertical solid gray lines separate the Leeuwin Current Extension, South Australian Current and Zeehan Current and the vertical dashed grey line separates the region with a zonal shelf to the west from the region with a slanted shelf to the east. The coloured numbers in (a) and (b) show, from left to right, the mean transport in the Leeuwin Current Extension region, the zonal South Australian Current region, the slanted South Australian Current region and the Zeehan Current region in summer (orange) and in autumn (purple). In (c) and (d), the magnitude of the Ekman drift is indicated by the shading whereas arrow lengths are proportional to the square root of the vector amplitudes. (For interpretation of the references to colour in this figure legend, the reader is referred to the web version of this article.)

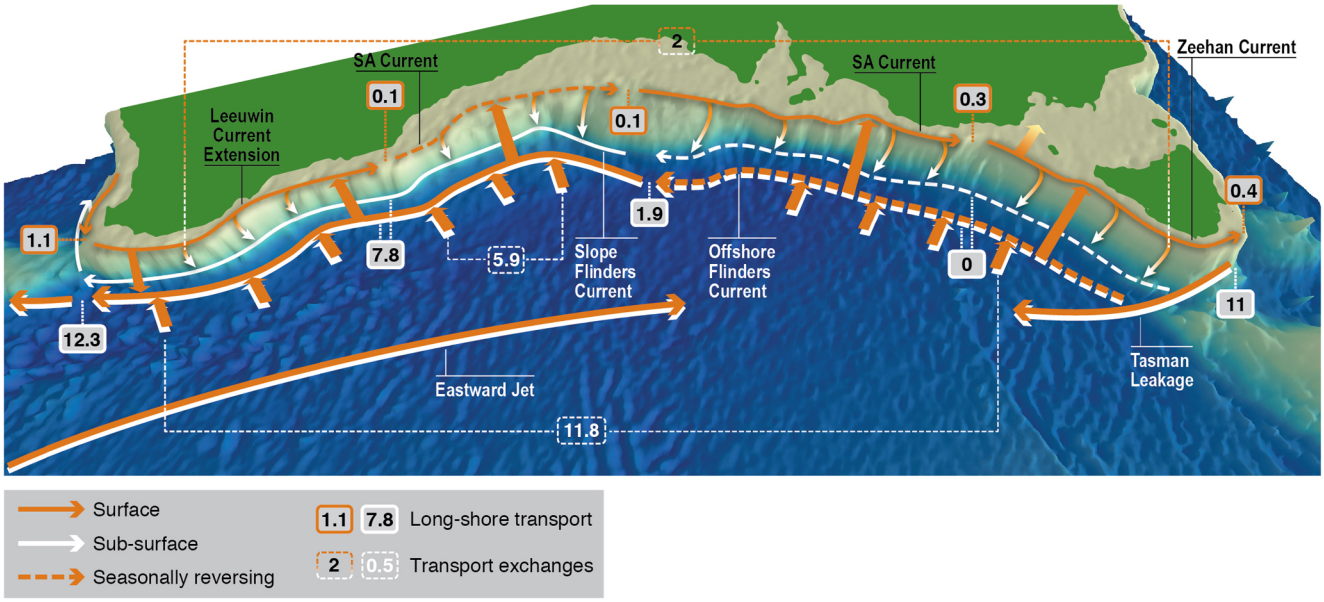

Fig. 10. Southern Australia Current System summary transport budget schematics. Long-shore transport for the SBC and FC in grey box with orange outline and white outline, respectively. Integrated vertical and onshore flows transport in dashed outline box. For visibility, white (black) text is overlaid on dark (light) background.

particularly in the Great Australian Bight (Fig. 9c). The strengthening of the SBC occurs in autumn when the westerlies start strengthening and shifting north as shown by the strong basin-wide onshore Ekman drift (Fig. 9d). Indeed, the SBC are strongest in autumn with an average eastward transport between 0.8 and 1.1 Sv and a maximum eastward transport up to 1.75 Sv (Fig. 9a).

The FC also displays a strong seasonal variability (Fig. 9b). In summer, the FC is strongest along both the slanted and the zonal shelf. Near the south-west corner of Australia, the FC carries on average 13.9 Sv westward, with maximum transport around 19 Sv. In autumn, the FC is weakest, eastward along the slanted shelf (average eastward transport up to 4.8 Sv), and westward along the zonal shelf with an average westward transport of 7.1 Sv off south-western Australia. The SBC and the FC therefore have a seasonally opposed strengthening–weakening cycle and the SBC–offshore-FC pairing is affected by the Ekman drift's seasonality. For instance the summer transport is dominated by the strongly westward FC with little to no eastward transport from the SBC. In autumn, the transport from the SBC is strongly eastward whereas the slanted FC is reversed. We expect that the SBC–slope-FC pairing via downwelling and onshore flows feeding into the FC would also exhibit a strong seasonality, which will be examined in a future study.

4. Summary

We investigated the structure, transport budget and coupling of currents in the Southern Australia Current System and have provided the first comprehensive description of the circulation along the southern shelves of Australia and the South Australian Basin. The Southern Australia Current System contains the eastward Shelf Break Currents (SBC, from west to east: Leeuwin Current Extension, South Australian Current and Zeehan Current), and the counter-flowing westward Flinders Current (FC) both offshore of, and underneath, the SBC. We separated the domain into a zonal sector between Cape Leeuwin (115°E) and the eastern Great Australian Bight (132°E) where the continental margin is approximately zonal, and a slanted sector between the eastern Bight and South East Cape south of Tasmania (147°E), where the margin is slanted. We conducted an identical analysis in CARS, a long-term average of hydrographic observations gridded at a 1/8° resolution and MOM01, a 7-year subset of a long-term OGCM simulation at a 1/10° resolution forced by a repeated climatological annual cycle of atmospheric conditions. We derived mass-conserving flows from temperature and salinity fields and defined the boundaries of the SBC and the FC to produce a closed transport budget. The purpose of this work was to synthesize past observational and modelling results into a comprehensive picture of the Southern Australia Current System. The agreement we find between the observations and the model provide confidence that the methodology used here and in Furue et al.'s (2017) can provide insight into other boundary circulations. This paper also aims to serve as groundwork for a future study on the seasonality and dynamical mechanisms of the system.

4.1. Southern Australia Current System structure

In general, the annual-mean SBC agreed well between CARS and MOM01 (Fig. 2 and 3). The SBC are confined to the upper 250 m with a maximum speed of 20 cm s^{-1}. The SBC are fairly continuous all along the shelf break (Fig. 3a,b and 6a) with a weakening Leeuwin Current Extension between Cape Leeuwin and Cape Carnot (124°E); a stable zonal South Australian Current between Cape Carnot and the eastern Great Australian Bight; a strengthening slanted South Australian Current between the eastern Bight and Portland (141°E) and an also strengthening Zeehan Current between Portland and South East Cape.

In general, the FC speed in CARS was in good agreement with individual observational records, and was stronger than in MOM01. The FC has a dual structure with a slope-FC core located along the continental slope around 600 m depth, which is an undercurrent for the SBC, and an offshore-FC core which is weak and patchy or even reverses along the slanted coast but becomes stronger and better defined in the zonal sector (Figs. 2 and 3).

There is a net downwelling from the lower and seaward portion of the SBC into the slope-FC in regions with a steep continental slope (Fig. 5). In one cross-shore section where the slope was significantly gentler, the slope-FC was absent and the SBC bottom flows were actually weakly upwelling. Generally, along the zonal shelf, the downwelling is weak (except off Cape Leeuwin, greater than -50×10^{-4} cm s^{-1}) and in the upper 600 m. Along the slanted shelf, the downwelling is strong (greater than -20×10^{-4} cm s^{-1}) and in the upper 1000 m.

These findings suggest that the downwelling from the SBC is important in maintaining the slope-FC which emerges along the slanted slope where the downwelling is strongest.

There is an eastward jet to the south of the offshore-FC, which is particularly well defined in the zonal sector (Fig. 3). This newly reported jet extends to 2000 m in the zonal sector (Fig. 2) and is weaker and confined to the upper 250 m in the slanted sector, where it bends south-eastwards along and into the slanted FC. This jet is probably an expression of the southern arm of the Albany High (see Introduction Section 1.3), a persistent regional anti-clockwise gyre centred offshore of Albany (118°E). With this interpretation, the zonal FC is the northern westward-flowing arm of the Albany High, and the eastward jet is the southern eastward-flowing arm.

4.2. Southern Australia Current System transport budget

The transport budget quantifies the spatial evolution of the annual-mean SBC and FC and the results are schematically summarized in Fig. 10.

The Leeuwin Current turns around the southwest corner of Australia to become, or feed into, the Leeuwin Current Extension. Its initial transport is 1.1 Sv eastward but it loses a part of its transport to downwelling and, to a lesser extent, to lateral offshore flows near Cape Leeuwin. The Leeuwin Current Extension eventually carries 0.1 Sv as it approaches the Great Australian Bight. The western South Australian Current flows along the zonal shelf break without substantial changes in transport. As the South Australian Current flows over the slanted shelf break, it receives more lateral inflow than the loss to downwelling and is consequently accelerated to 0.3 Sv. The Zeehan Current grows under the same process to 0.4 Sv where lateral inflows are strong enough to overcome both downwelling and a loss into Bass Strait. Overall, the SBC transport decrease from Cape Leeuwin to South East Cape is due to a $\mathscr{V}_{\mathrm{SBC}} = +1.5$ Sv lateral inflow from the FC, which is in turn downwelled as $\mathscr{W}_{\mathrm{SBC}} = -2$ Sv that then feeds back into the FC, and a $\mathscr{V}_{\mathrm{CC}} = -0.2$ Sv shallow lateral loss into Bass Strait.

The annual-mean FC is weak or absent off the western Tasmanian shelf and Bass Strait as the Tasman Leakage carries -11 Sv into the South Australian Basin interior with no direct retroflection into the FC off western Tasmania in our transport budget. The onshore flows along the slanted shelf are weak and result in only a weak increase to the FC transport (1.9 Sv) in the eastern Great Australian Bight. When the shelf becomes zonal, the onshore flows are much stronger and accelerate the FC to 7.8 Sv by Cape Carnot (the western end of the Bight) and to 12.3 Sv by Cape Leeuwin. Overall, 20.5% of the net onshore flows occur along the slanted shelf, 50% (-5.9 Sv) in the zonal Great Australian Bight, and 29.7% in the zonal shelf region from Cape Carnot to Cape Leeuwin. Therefore, nearly 80% of the onshore flow contribution to the FC increase occurs along the zonal shelf. Another $+0.5$ Sv net gain from the SBC comes from downwelling, which accounts for only about 4.1% of the FC's total increase.

4.3. Closing discussion

The continuity of the near-surface shelf break currents extending from Northwest Cape off Western Australia to Southeast Cape off Tasmania has been understood since Ridgway and Condie (2004) described them as a 5500 km long boundary current. The two components are the Leeuwin Current System off Western Australia and the collection of currents south of Australia that we here define as the Southern Australia Current System. The volume transport and spatial variability of the Leeuwin Current System was quantified in Furue et al. (2017). Here, we have adapted their method to quantify the transport and spatial variability of the Southern Australia Current System. The system consists of the eastward SBC and counter-flowing westward FC that has a slope-trapped part forming an undercurrent to the SBC, and a deep-reaching offshore part.

The dual analysis of observations and model in this study goes beyond the traditional approach of validating a model based on a range of indices available from observations, and then analyzing spatial and temporal variability using the model alone. We find here that applying identical methods to both model and observations, leads to enhanced confidence in the structure and transport of the Southern Australia Current System.

In this work, we have discovered a coupling between the SBC and slope-FC through downwelling, and between the SBC and offshore-FC through onshore Ekman drift. The annual-mean Ekman drift is largely onshore along the Southern Australian shelves (Fig. 7). In the Great Australian Bight and in front of the Spencer and St Vincent Gulfs, the Ekman drift curls anti-clockwise resulting in weaker onshore Ekman drift. The onshore Ekman drift supplies downwelling flows that are strongest where the shelf is steep, which is everywhere outside of the Great Australian Bight (Fig. 8).

The combined effect of the horizontally coupled SBC–offshore-FC pair and vertically coupled SBC–slope-FC pair is a conversion of some of the widespread northward Ekman drift into downwelling, with little impact on the horizontal transport of the SBC. A larger part of the onshore Ekman flow into the FC is directly converted into increasing the FC's westward transport from close to zero along western Tasmania to 12.3 Sv near the western side of Australia.

The SBC–slope-FC pair bears a striking similarity with the Leeuwin-Current–Leeuwin-Undercurrent (LC–LUC) pair described in Furue et al. (2017). The LC–LUC pair is driven the onshore geostrophic flow due to the meridional density gradient in the southeast Indian Ocean, and the SBC–slope-FC pair is driven by onshore Ekman drift. From the annual-mean perspective, the dynamical balance of both systems could be the same, with strong onshore flows being overturned into an undercurrent.

While this work has focused on the mean structure of the Southern Australia Current System, its temporal variability is of major interest for future work. Ridgway and Godfrey (2015) for example examined the seasonal cycle of the Leeuwin Current System and found that annual pressure signals originating from north of Australia propagate around Australia counter-clockwise, reaching to Tasmania. In the present paper, a brief analysis of the SBC and FC summer and autumn states showed that the SBC–offshore-FC pairing via Ekman drift is significantly modified by the Ekman drift's seasonality. In summer, the Ekman drift is mostly oriented offshore which drives weak SBC that are reversed to westward in some places, particularly in the Great Australian Bight where the zonal South Australian Current flows (Fig. 10). In contrast, the FC is at its strongest in summer, transporting up to 19 Sv westward. In autumn, the Ekman drift is stronger and oriented onshore due to a strengthening and northward shift of the westerly winds in this season. This drives strong SBC with an eastward transport up to 1.75 Sv, while the FC is at its weakest and reversed along the slanted shelf (Fig. 10).

In the Leeuwin Current System, the Leeuwin Current undergoes a seasonal cycle (Ridgway and Godfrey, 2015) but does not strongly reverse like the zonal South Australian Current does in summer, or the slanted FC does in autumn. In the domain of the present study, there is a significant seasonal cycle in winds, which contributes to the seasonal cycle of the SBC and the FC and is likely to contribute to seasonality in other aspects of the Southern Australia Current System such as the SBC–slope-FC pairing via downwelling and the onshore flows feeding into the FC. This will be the focus of a future study.

Slower timescale variability in this boundary current system is also of interest. For example, Feng et al. (2003) documented the impact of ENSO on the transport variability of the Leeuwin Current System. A prevailing La Niña state was found to be a key contributor to the devastating 2011 marine heat wave off Western Australia (Feng et al., 2013). The impact on the Southern Australia Current System of large-scale climate modes, such as ENSO and the Southern Annular Mode, and their impact on marine climate along the southern Australian coastline have yet to be defined. The consistency between CARS and the

MOM01 model in this work suggests that the model is well suited to investigating these questions. New observations of this under-sampled boundary current are essential to ground-truth the model results.

Declaration of Competing Interest

The authors declare that they have no known competing financial interests or personal relationships that could have appeared to influence the work reported in this paper.

Acknowledgment

This study was supported by the Australian Research Council Discovery Projects (DP130102088) and by the National Science Foundation through Grant OCE-0961716. We thank Jeff Dunn for updating the CARS Aus8 dataset (http://www.marine.csiro.au/atlas/). ERA-Interim data is publicaly available on https://www.ecmwf.int/en/forecasts/datasets/archive-datasets/reanalysis-datasets/era-interim. MOM01 data is publicaly available on http://cosima.org.au/index.php/models/access-om2-01-2/. ED thanks the Consortium for Ocean-Sea Ice Modelling in Australia (COSIMA, http://cosima.org.au) and the Australian National Computing Infrastructure for making the MOM01 run possible. This work benefited from discussions with Matthew England. ED was supported by the Australian Research Council Centre of Excellence for Climate System Science. HP and NB acknowledge funding from the Australian Government's National Environmental Science Programme. RF was partially supported by the Japan Society for the Promotion of Science through KAKENHI 16K05562. Funding from the ARC Centre of Excellence for Climate Systems Science and the University of Tasmania enabled RF to visit the lead author's institute. PS was supported by an Australian Research Council (ARC) DECRA Fellowship DE150100223.

Appendix A. Geostrophic velocity derivation

A.1. Helland-Hansen method and Ekman drift calculation

To compute geostrophic velocities in regions shallower than the reference depth, we apply the Helland-Hansen method (Helland-Hansen, 1934; Fomin, 1964). This method states velocities at the bottom of a land portion shallower than the reference depth are zero. We first compute geostrophic velocities referenced to the surface and then remove a vertically-uniform velocity field that cancels out the geostrophic velocities at the reference depth in the ocean interior or at the sea bottom over the margin; hence

$$\mathbf{V}_g^* = \mathbf{V}_0 - \mathbf{V}_0(z = z_{HH}), \tag{A.1}$$

where $z \in [-2000\ \text{m}, 0]$ is the local depth, $z_{HH} = \max(z_{ref}, z_b)$ is a depth that corresponds to the shallowest level between z_{ref} and the local sea bottom depth $z_b(x, y)$, $\mathbf{V}_0 = (u_0, v_0)$ are the geostrophic velocities referenced to the surface and $\mathbf{V}_{g^*}$ are the geostrophic velocities from the Helland-Hansen method.

To account for the wind effect at the surface we calculate the Ekman drift $\mathbf{V}_{ek}$ (m^2s^{-1}) as

$$\mathbf{V}_{ek} = -\mathbf{k} \times \frac{\tau}{f\rho_0}, \tag{A.2}$$

where $\mathbf{k}$ is an upward pointing unit vector, $\tau = (\tau^x, \tau^y)$ is the wind stress, f is the Coriolis parameter and ρ_0 is a constant mean density. Note that in the geostrophic calculation, we assume that the bottom is slippery and therefore there is no Ekman drift at the bottom.

A drawback of the Helland-Hansen method is that it produces large vertical flows across the sea bottom over the margin, which introduces error in three-dimensional transport budgets. These cross-bottom leaks are evident from high divergence values in the depth-integrated velocity field, $\nabla\cdot\mathbf{V}^*$ (not shown). This depth-integrated velocity field $\mathbf{V}^* = \mathbf{V}_{g^*} + \mathbf{V}_{ek}$ is the sum of contributions from both geostrophy and Ekman drift and is defined as

$$\mathbf{V}^* = \int_{z_{HH}}^{0} \mathbf{v}_g^*\, dz + \mathbf{V}_{ek}. \tag{A.3}$$

To eliminate this deficiency, we apply the Zero-Divergence method described in Furue et al. (2017) and in Appendix A.2.

A.2. Zero-divergence method

Here, we remove a second barotropic velocity field $\mathbf{V}_d = \nabla\phi$ from $\mathbf{V}^*$ such that $\nabla\cdot(\mathbf{V}^* - \nabla\phi) = 0$, so that ϕ satisfies the Poisson equation

$$\nabla^2\phi = \nabla\cdot\mathbf{V}^*. \tag{A.4}$$

We solve the above equation by setting a no-flow condition on $\mathbf{V}_d$ everywhere at the solid land and open ocean boundaries except along the southern open ocean boundary. At the southern boundary we set $\phi = 0$ there to allow for a net inflow or outflow of $\mathbf{V}_d$ to compensate for the total divergence $\iint \nabla\cdot\mathbf{V}^* dx\, dy$. In order to ensure the impact of that weak artificial flow over the Southern Australia Current System is minimal, we set the open boundary 2° south of our domain, along 50°S. The resulting adjusted geostrophic field $\mathbf{v}_g$ is expressed as

$$\mathbf{v}_g = \mathbf{v}_g^* - \frac{\mathbf{V}_d}{-z_{HH}}, \tag{A.5}$$

where $\nabla\cdot\mathbf{V} = \nabla\cdot\left(\int_{z_{HH}}^{0} \mathbf{v}_g\, dz + \mathbf{V}_{ek}\right) = 0$ everywhere including over the continental shelf and slope.

Appendix B. SBC and FC lateral boundary definition

Since the SBC and FC are strongly topographically controlled, we define their northern and southern boundaries by working along two isobaths: one that best follows the SBC and another one that best follows the FC. In the upper layer (Fig. 3a), the SBC's northern (southern) boundary is defined as some degrees north (south) of their isobath depending on the current's cross-shore width. The FC's northern boundary is defined as the SBC's southern boundary in the upper layer and as the continental slope in the lower layer (Fig. 3b). The FC's southern boundary is defined as some degrees south of its isobath depending on the current's seaward extent.

Since the shelf orientation varies, we increase the distance between the SBC's northern and southern boundaries when the shelf is more slanted to

ensure the SBC are fully captured. West of Portland, we select the 700 m isobath for the SBC and define y_{CC} to be 3/8° to the north and y_{int} to be 3/8° to the south. East of Portland, where the shelf break is meridional, we define y_{CC} to be 1/2° to the north and y_{int} to be 3/4° to the south of the 700 m isobath. South of Tasmania, where the coastline is zonal, y_{int} is 3/8° to the south of the isobath again. We remove y_{CC} where the shallow shelf is narrow and the coastal currents are insignificant, that is anywhere outside the Great Australian Bight, the Bass Strait, the Gulfs region north of Cape Jaffa. Finally, we define the FC's southern boundary y_{OF} by following the 2000 m isobath. West of Portland y_{OF} is set to be 3/2° south of this isobath. Elsewhere, it is set to be 7/4° south. South of Tasmania, the boundary is manually adjusted to lie at 45.5°S. The green, red and magenta curves in Fig. 3 are y_{CC}, y_{int} and y_{OF} as defined above.

We note MOM01 shows continuous SBC well incorporated into the SBC control volume (Fig. 3c). Even though CARS is a long-term climatology, it still includes some coastal eddy-like "noise" in the region (Fig. 3a), which is likely due to the superposition of eddies recorded at different times. Recently, Oke et al. (2018) found that the Great Australian Bight is rich in mesoscale eddies with surface-intensified currents coherent over the water column. The eddies, which are hypothetically due to the horizontal shear associated with the SBC, are most energetic when the SBC seasonally weaken. In MOM01, the eddies synoptic structure, particularly in the Leeuwin Current Extension region, is evident on transient timescales (not shown). Defining fixed boundaries around the SBC is, however, adequate, because the long-term mean boundary circulation is mostly dominated by geostrophic flows. The SBC's jet like shape is maintained by southward propagating pressure anomalies from the Leeuwin Current System. These pressure anomalies turn eastward along southern Australia (Middleton and Bye, 2007; Ridgway and Godfrey, 2015). In winter, the currents are reinforced due to westerly winds intensification and increased onshore Ekman drift (Ridgway and Condie, 2004). In our fixed boundary SBC definition, any eddies and eddy-like meandering flows crossing a boundary will be captured as an inflow or outflow into the currents. Furue et al. (2017) also applied fixed boundaries for the Leeuwin Current System, because the Leeuwin Current, which co-exists with eddies, is also a jet-like flow.

Appendix C. On the definition of longshore transport

This appendix discusses the definition of the transport for a longshore current. In the main text, we integrate zonal velocity instead of longshore velocity to define the transport of the SBC or FC (Section 2.4) Here we explain why our volume-conserving approach is the best method to use.

C.1. On using gridboxes to construct the control volume for leak-free calculations

The central part of this study is to develop a transport budget for the Southern Australia Current System. To do this, it is essential that the currents are captured by control volumes with horizontal and vertical boundaries that fully enclose the currents. Details of this are provided in Section 2.3.

Once the control volumes of the currents are defined, we can use conservation of mass to derive the transports of the longshore current by adding all the horizontal and vertical transports across the faces of the control volumes. The faces of our control volumes are set to coincide with faces of the underlying gridboxes. This arrangement enables an exact closure of volume budget except for the tiny truncation error at machine precision with a relative error of the order of 10^{-14} or less (Furue, 2019). This property is shown in Fig. C.1 where we made a difference of the zonal transport of a current (SBC is the left panel and FC is the right panel) between the actual zonal transport, which was calculated by integrating U along each meridional slice within a control volume (left-hand side of Eq. (11) or (12)), and the zonal transport calculated by accumulating sources/sinks upstream of the meridional slice (right-hand side of Eq. (11) or (12)). Fig. C.1 shows the high-accuracy of our method and demonstrates that our budget closes to computer precision.

Since the volume budget closes to a high precision, it is evident that the longshore transport across a section can be determined by accumulating the lateral and vertical transports across the faces of the control volume upstream of the section, regardless of the orientation of the section (Fig. 2).

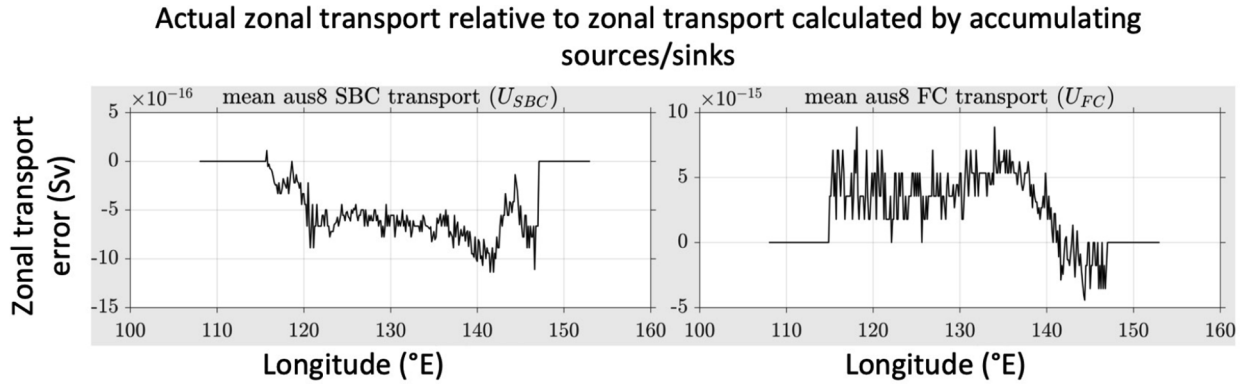

Fig. C.1. Zonal transport error in Sv for the SBC (left) and the FC (right) showing the differences between the left-hand and right-hand sides of Eqs. (A.4) and (A.5).

C.2. On using meridional sections rather than normal sections

The most straightforward orientation of the section is meridional because the section then automatically follows faces of our classical lat-lon gridboxes. Next, we use Fig. C.2 to explain the differences between meridional slicings and slicings normal to the coast.

C.2.1. On the difference between the zonal transport and the longshore transport

Where the shelf is oriented zonally (Case 1 in Fig. C.2), the meridional slices are normal to the coast. If we were to slice the volume perpendicularly to the slanted coast (Case 2 Fig. C.2), this would result in a situation equivalent to Case 1. In Case 3 of Fig. C.2, meridional slices along the slanted coast (thick black lines) are longer than if they were normal to the coast (thick gray lines). Despite this difference, the volume transports

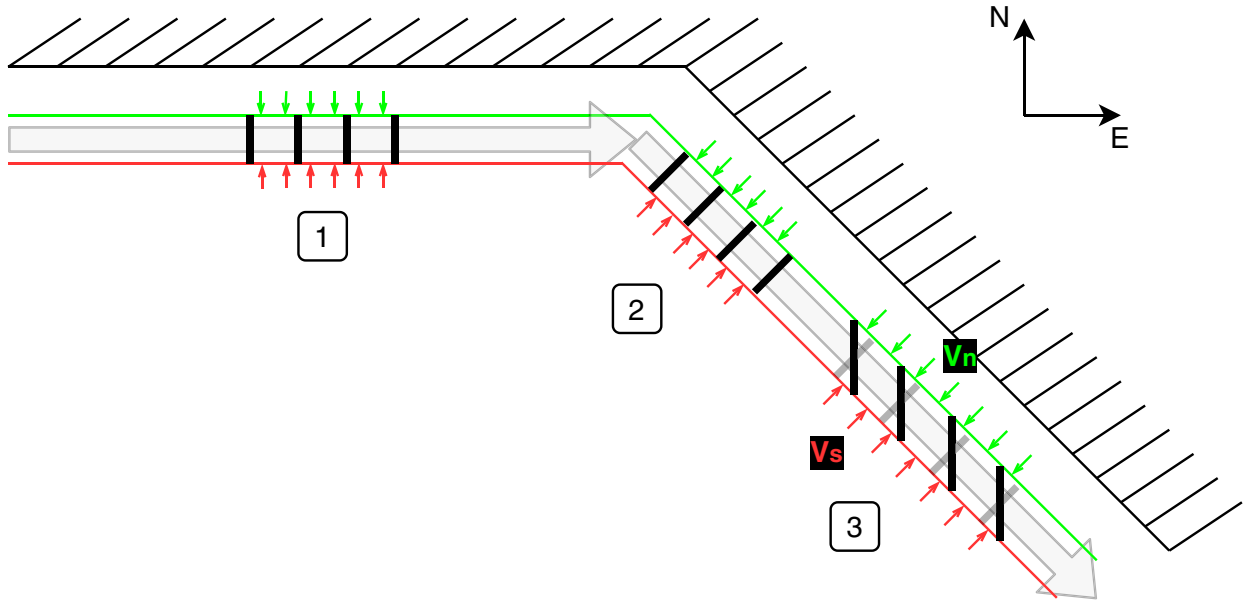

Fig. C.2. Simplified schematics of the SBC (wide arrows) along a zonal shelf and a slanted shelf. The SBC is bounded to the north by the green line and to the south by the red line. The thin coloured arrows show the horizontal cross-boundary transports into the SBC across the north face (V_n) and south (V_s) of the SBC (we assume these transports to be into the SBC for simplicity). There is also an implied vertical transport across the bottom face of the SBC volume which we do not represent here for simplicity. V_n and V_s are the lateral transports across the north and south faces of the current, respectively. The slicing across the SBC volume is shown as thick lines. Case 1 shows meridional slices along a zonal shelf. Case 2 shows normal slices along a slanted shelf. Case 3 shows meridional slices along a slanted shelf (thick black lines) and normal slices along a slanted shelf (thick semi-transparent gray lines).

across the two slices can be different only by lateral inflows across the sides of the little triangles formed by these two slices and by the vertical transports across the bottom faces of the triangles as shown below. In Fig. C.2 and in the below equation we only consider the lateral inflows for simplicity.

If $\widehat{\mathscr{U}}$ is the transport across the meridional slices and $\mathscr{U}$ is the transport across the slices normal to the coast, then

$$\widehat{\mathscr{U}} = \mathscr{U} + V_n dl_n - V_s dl_s, \tag{C.1}$$

where V_n is the inflow across the north face of the current (Fig. C.2), dl_n is the length along the north face between a meridional slice and a normal slice, V_s is the inflow across the south face of the current (Fig. C.2), dl_s is the length along the south face between the meridional slice and the normal slice.

Hence, for a given meridional slice, some extra flows across the north face equivalent to $V_n dl_n$ are included in the current transport and some flows across the south face equivalent to $V_s dl_s$ are not included in the current transport, in comparison to a normal slice. When the current is wider, dl_n and dl_s become accordingly longer and the difference between $\mathscr{U}$ and $\widehat{\mathscr{U}}$ tends to be larger (depending on the signs and sizes of V_n and V_s).

C.2.2. On the difference between zonal transport and longshore transport in the Southern Australia Current System case

An implication of the above discussion is that, while it is true that volume transports with meridional slices will be different to volume transports with normal slices where the shelf is slanted, the difference between the meridional slicing and the normal slicing will be minimal provided:

- that the slant is not too meridional. If the slant is too meridional, the sides of the little triangles (Case 3 in Fig. C.2) rapidly grow and the two volume transports ($\mathscr{U}$ and $\widehat{\mathscr{U}}$) diverge; and
- that the currents are narrow. If the currents are too wide, the sides of the little triangles will also be too long.

In Fig. C.3 we show a faded, zoomed-in version of Fig. 3c where we added meridional and normal slices for the FC in a few selected regions. We can see that the triangles resulting from the tilt difference between meridional and normal slices increase in size where the current is wider (e.g. western most slices) and where the slant is stronger (e.g. eastern most slices). Given the narrowness of the SBC, the difference between meridional slices and normal slices will be minimal and is not shown in the figure. For the FC, there may be some local differences where the current gets wider or where the slant is stronger (west of Tasmania). These local differences are acceptable because in this paper we do not try to make precise comparisons of our transport values with other estimates at each point for the FC or SBC. Rather we intend to show how these currents' transports vary along the coast. Unless we compare our transport values directly with cross-shore observations, the difference $\widehat{\mathscr{U}} - \mathscr{U} = V_n dl_n - V_s dl_s$ is immaterial because our volume budget analysis is self-consistent and leak-free. For all the reasons discussed above, we used the zonal transport for the transport of the currents.

Even if we wanted to calculate a transport like $\mathscr{U}$ above, defining a cross-shore section is not straightforward given that the coast line is not a smooth curve. Then, if all sections follow outlines of grid-boxes, leak-free calculations are feasible, but in this case, each section would have to be defined manually. If, on the other hand, the sections are allowed to intersect grid-boxes, remapping the velocity field in such a way that the total volume is conserved would be very difficult and beyond the scope of this work.

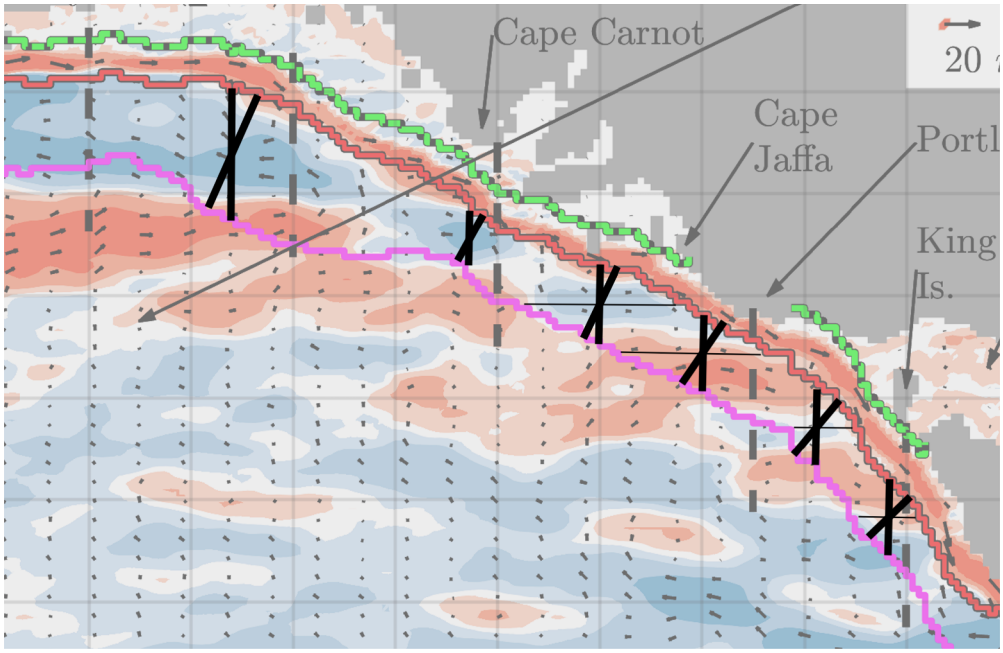

Fig. C.3. Faded and zoomed-in version of Fig. 3c. Some examples of meridional and normal slices are shown as thick black lines. The difference between meridional slices and normal slices is shown by the triangles resulting from the tilt difference between the two slices. Zonal slices where the shelf is more slanted are shown as thin black lines. The normal slices are drawn by eye for illustrative purposes.

References

Anderson, D.L., Gill, A., 1975. Spin-up of a stratified ocean, with applications to upwelling. Deep Sea Res. Oceanographic Abst. 22 (9), 583–596. https://doi.org/10.1016/0011-7471(75)90046-7.

Baines, P.G., Edwards, R.J., Fandry, C.B., 1983. Observations of a New Baroclinic current along the western continental-slope of bass strait. Aust. J. Mar. Freshw. Res. 34 (1), 155–157.

Batteen, M.L., Miller, H.A., 2009. Process-oriented modeling studies of the 5500-km–long boundary flow off western and southern Australia. Cont. Shelf Res. 29 (4), 702–718. https://doi.org/10.1016/j.csr.2008.11.011.

Batteen, M.L., Kennedy, R.A., Miller, H.A., 2007. A process-oriented numerical study of currents, eddies and meanders in the Leeuwin Current System. Deep Sea Res. II 54 (8–10), 859–883. https://doi.org/10.1016/j.dsi2.2006.09.006.

Cetina-Heredia, P., van Sebille, E., Matear, R.J., Roughan, M., 2018. Nitrate Sources, Supply, and Phytoplankton Growth in the Great Australian Bight: An Eulerian-Lagrangian Modeling Approach. J. Geophys. Res.: Oceans 123 (2), 759–772. https://doi.org/10.1002/2017JC013542.

Chaudhuri, A.H., Ponte, R.M., Forget, G., Heimbach, P., 2013. A comparison of atmospheric reanalysis surface products over the ocean and implications for uncertainties in air-sea boundary forcing. J. Clim. 26 (1), 153–170. https://doi.org/10.1175/JCLI-D-12-00090.1.

Cirano, M., Middleton, J.F., 2004. Aspects of the mean wintertime circulation along Australia's southern shelves: Numerical studies. J. Phys. Oceanogr. 34 (3), 668–684.

Cleveland, W.S., Devlin, S.J., 1988. Locally weighted regression: an approach to regression analysis by local fitting. J. Am. Stat. Assoc. 83 (403), 596–610. https://doi.org/10.1080/01621459.1988.10478639.

Cresswell, G., 2000. Currents of the continental shelf and upper slope of Tasmania. Pap. Proc. R. Soc. Tasmania 133, 21–30.

Cresswell, G., Peterson, J., 1993. The Leeuwin current south of Western Australia. Marine Freshwater Res. 44 (2), 285–303. https://doi.org/10.1071/MF9930285.

Cresswell, G.R., Griffin, D.A., 2004. The Leeuwin Current, eddies and sub-Antarctic waters off south-western Australia. Marine Freshwater Res. 55 (3), 267–276.

Dee, D.P., Uppala, S.M., Simmons, A.J., Berrisford, P., Poli, P., Kobayashi, S., Andrae, U., Balmaseda, M.A., Balsamo, G., Bauer, P., Bechtold, P., Beljaars, A.C.M., van de Berg, L., Bidlot, J., Bormann, N., Delsol, C., Dragani, R., Fuentes, M., Geer, A.J., Haimberger, L., Healy, S.B., Hersbach, H., Holm, E.V., Isaksen, L., Kallberg, P., Kohler, M., Matricardi, M., McNally, A.P., Monge-Sanz, B.M., Morcrette, J.J., Park, B.K., Peubey, C., de Rosnay, P., Tavolato, C., Thepaut, J.N., Vitart, F., 2011. The ERA-Interim reanalysis: configuration and performance of the data assimilation system. Quart. J. Roy. Meteorol. Soc. 137 (656), 553–597.

Duran, E., 2015. An investigation of the Leeuwin Undercurrent source waters and pathways. Ph.D thesis. University of Tasmania.

Feng, M., Meyers, G., Pearce, A., Wijffels, S., 2003. Annual and interannual variations of the Leeuwin Current at 32 degrees S. J. Geophys. Res.-Oceans 108 (C11).

Feng, M., McPhaden, M.J., Xie, S.-P., Hafner, J., 2013. La Niña forces unprecedented Leeuwin Current warming in 2011. Sci. Rep. 3, 1277.

Feng, M., Zhang, X.B., Oke, P., Monselesan, D., Chamberlain, M., Matear, R., Schiller, A., 2016. Invigorating ocean boundary current systems around Australia during 1979–2014: As simulated in a near-global eddy-resolving ocean model. J. Geophys. Res.-Oceans 121 (5), 3395–3408.

Fomin, L.M., 1964. The Dynamic Method in Oceanography, Elsevier Oceanography Series. Elsevier Pub. Co., Amsterdam, New York.

Furue, R., 2019. The three-dimensional structure of the Leeuwin Current System in density coordinates in an eddy-resolving OGCM. Ocean Model. 138, 36–50. https://doi.org/10.1016/j.ocemod.2019.03.001.

Furue, R., Guerreiro, K., Phillips, H.E., McCreary, J.P., Bindoff, N.L., 2017. On the Leeuwin current system and its linkage to zonal flows in the South Indian ocean as inferred from a gridded hydrography. J. Phys. Oceanogr. 47 (3), 583–602. https://doi.org/10.1175/jpo-d-16-0170.1.

Garrey, J., Maxwell, H., Cresswell, G.R., 1981. Dispersal of tropical marine fauna to the great australian bight by the Leeuwin current. Aust. J. Mar. Freshw. Res. 32 (4), 493–500.

Godfrey, J.S., Ridgway, K.R., 1985. The large-scale environment of the poleward-flowing Leeuwin current, Western-Australia - Longshore steric height gradients, wind stresses and geostrophic flow. J. Phys. Oceanogr. 15 (5), 481–495.

Godfrey, J.S., Vaudrey, D.J., Hahn, S.D., 1986. Observations of the Shelf-Edge Current South of Australia, Winter 1982. J. Phys. Oceanogr. 16 (4), 668–679.

Griffies, S.M., 2012, Elements of the Modular Ocean Model (MOM): 2012 release with updates. Tech. rep., GFDL/NOAA.

Helland-Hansen, B. 1934. The Sognefjord section: Oceanographic observations in the northernmost part of the North Sea and the southern part of the Norwegian Sea. In: James Johnstone Memorial Volume, Liverpool Univ Press, pp. 257–274.

Hufford, G.E., McCartney, M.S., Donohue, K.A., 1997. Northern boundary currents and adjacent recirculations off southwestern Australia. Geophys. Res. Lett. 24 (22), 2797–2800. https://doi.org/10.1029/97GL02278.

Huthnance, J.M., 1995. Circulation, exchange and water masses at the ocean margin: the role of physical processes at the shelf edge. Prog. Oceanogr. 35 (4), 353–431. https://doi.org/10.1016/0079-6611(95)80003-C.

Large, W.G., Yeager, S.G., 2009. The global climatology of an interannually varying air-sea flux data set. Clim. Dyn. 33 (2–3), 341–364.

Legeckis, R., Cresswell, G., 1981. Satellite-observations of sea-surface temperature fronts off the coast of western and Southern Australia. Deep-Sea Res. Part a-Oceanograp. Res. Pap. 28 (3), 297–306.

McCartney, M.S., Donohue, K.A., 2007. A deep cyclonic gyre in the Australian-Antarctic Basin. Prog. Oceanogr. 75 (4), 675–750.

McClatchie, S., Middleton, J.F., Ward, T.M., 2006. Water mass analysis and alongshore variation in upwelling intensity in the eastern Great Australian Bight. J. Geophys. Res. 111 (C8), C08,007. https://doi.org/10.1029/2004JC002699.

McCreary, J.P., 1981. A linear stratified ocean model of the equatorial undercurrent. Philosoph. Trans. Roy. Soc. A: Mathe., Phys. Eng. Sci. 298 (1444), 603–635. https://doi.org/10.1098/rsta.1981.0002.

McCreary, J.P., Fukamachi, Y., Kundu, P.K., 1991. A numerical investigation of jets and eddies near an eastern ocean boundary. J. Geophys. Res.: Oceans 96 (C2), 2515–2534. https://doi.org/10.1029/90JC02195.

McCreary, J.P., Kundu, P.K., Molinari, R.L., 1993. A numerical investigation of dynamics, thermodynamics and mixed-layer processes in the indian-ocean. Prog. Oceanogr. 31 (3), 181–244. https://doi.org/10.1016/0079-6611(93)90002-u.

Middleton, J.F., Bye, J.A.T., 2007. A review of the shelf-slope circulation along Australia's southern shelves: Cape Leeuwin to Portland. Prog. Oceanogr. 75 (1), 1–41. https://

doi.org/10.1016/j.pocean.2007.07.001.
Middleton, J.F., Cirano, M., 2002. A northern boundary current along Australia's southern shelves: The Flinders Current. J. Geophys. Res.-Oceans 107 (C9). https://doi.org/10.1029/2000jc000701. Artn 3129.
Middleton, J.F., Platov, G., 2003. The mean summertime circulation along Australia's southern shelves: A numerical study. J. Phys. Oceanogr. 33 (11), 2270–2287.
Oke, P.R., Griffin, D.A., Rykova, T., de Oliveira, H.B., 2018. Ocean circulation in the Great Australian Bight in an eddy-resolving ocean reanalysis: The eddy field, seasonal and interannual variability. Deep Sea Res. Part II 157–158, 11–26. https://doi.org/10.1016/j.dsr2.2018.09.012.
Oliver, E.C., Herzfeld, M., Holbrook, N.J., 2016. Modelling the shelf circulation off eastern Tasmania. Cont. Shelf Res. 130, 14–33. https://doi.org/10.1016/j.csr.2016.10.005.
Oliver, E.C.J., Holbrook, N.J., 2018. Variability and long-term trends in the shelf circulation off eastern Tasmania. J. Geophys. Res.: Oceans 123 (10), 7366–7381. https://doi.org/10.1029/2018JC013994.
Pennel, R., Stegner, A., Béranger, K., 2012. Shelf impact on buoyant coastal current instabilities. J. Phys. Oceanogr. 42 (1), 39–61. https://doi.org/10.1175/JPO-D-11-016.1.
Ridgway, K.R., 2007. Seasonal circulation around Tasmania: An interface between eastern and western boundary dynamics. J. Geophys. Res.-Oceans 112 (C10).
Ridgway, K.R., Condie, S.A., 2004. The 5500-km-long boundary flow off western and southern Australia. J. Geophys. Res.-Oceans 109 (C4). https://doi.org/10.1029/2003jc001921. C04,017.
Ridgway, K.R., Godfrey, J.S., 2015. The source of the Leeuwin Current seasonality. J. Geophys. Res.: Oceans 120 (10), 6843–6864.
Ridgway, K.R., Dunn, J.R., Wilkin, J.L., 2002. Ocean interpolation by four-dimensional weighted least squares—Application to the waters around Australasia. J. Atmospheric Oceanic Technol. 19 (9), 1357–1375.
Rochford, D.J., 1986. Seasonal-changes in the distribution of Leeuwin current waters off Southern Australia. Aust. J. Mar. Freshw. Res. 37 (1), 1–10.
Rosell-Fieschi, M., Rintoul, S.R., Gourrion, J., Pelegrí, J.L., 2013. Tasman Leakage of intermediate waters as inferred from Argo floats. Geophys. Res. Lett. 40 (20), 5456–5460. https://doi.org/10.1002/2013GL057797.
Smith, W., Sandwell, D., 1997. Global sea floor topography from satellite altimetry and ship depth soundings. Science.
Speich, S., Blanke, B., de Vries, P., Drijfhout, S., Doos, K., Ganachaud, A., Marsh, R., 2002. Tasman leakage: A new route in the global ocean conveyor belt. Geophys. Res. Lett. 29 (10), 4. https://doi.org/10.1029/2001gl014586.
Stewart, K., Hogg, M.A., Griffies, S., Heerdegen, A., Ward, M., Spence, P., England, M., 2017. Vertical resolution of baroclinic modes in global ocean models. Ocean Model. 113, 50–65.
Thompson, R.O.R.Y., Veronis, G., 1983. Poleward boundary current off Western Australia. Aust. J. Mar. Freshw. Res. 34 (1), 173–185.
van Sebille, E., England, M.H., Zika, J.D., Sloyan, B.M., 2012. Tasman leakage in a fine-resolution ocean model. Geophys. Res. Lett. 39, 5. https://doi.org/10.1029/2012gl051004.
van Sebille, E., Sprintall, J., Schwarzkopf, F.U., Sen Gupta, A., Santoso, A., England, M.H., Biastoch, A., Boning, C.W., 2014. Pacific-to-Indian Ocean connectivity: Tasman leakage, Indonesian Throughflow, and the role of ENSO. J. Geophys. Res.-Oceans 119 (2), 1365–1382. https://doi.org/10.1002/2013jc009525.
Woo, M., Pattiaratchi, C., 2008. Hydrography and water masses off the Western Australian coast. Deep-Sea Res. Part I-Oceanographic Res. Pap. 55 (9), 1090–1104. https://doi.org/10.1016/j.dsr.2008.05.005.
Yit Sen Bull, C., van Sebille, E., 2016. Sources, fate, and pathways of Leeuwin Current water in the Indian Ocean and Great Australian Bight: A Lagrangian study in an eddy-resolving ocean model. J. Geophys. Res.: Oceans 121 (3), 1626–1639. https://doi.org/10.1002/2015JC011486.